Collision induced absorption in HITRAN2024: Enhanced and improved data for atmospheric and planetary studies

J. Terragni, I.E. Gordon, E.M. Adkins, C. Boulet, A. Campargue, D. Chistikov, A. Finenko, H. Finkenzeller, H. Fleurbaey, R.J. Hargreaves, et al.

Highlights

Collision Induced Absorption in HITRAN2024: Enhanced and Improved Data for Atmospheric and Planetary Studies

J. Terragni, I. E. Gordon, E. Adkins, C. Boulet, A. Campargue, D. Chistikov, A. Finenko, H. Finkenzeller, H. Fleurbaey, R. J. Hargreaves, R. K. Hanson, J.-M. Hartmann, Andrew Klingberg, E. Kohler, A. O. Koroleva, D. Mondelain, G. Piccioni, S. Stefani, C. L. Strand, H. Tran, M. Turbet, A. Vigasin, F. Vitali, R. Volkamer, C. Wei

- Highlight 1
- Highlight 2
- Highlight 3

Collision Induced Absorption in HITRAN2024: Enhanced and Improved Data for Atmospheric and Planetary Studies

J. Terragni[a,*], I. E. Gordon[b], E. Adkins[j], C. Boulet[l], A. Campargue[c], D. Chistikov[n,o], A. Finenko[n,o], H. Finkenzeller[h], H. Fleurbaey[c], R. J. Hargreaves[b], R. K. Hanson[g], J.-M. Hartmann[d], Andrew Klingberg[g], E. Kohler[a], A. O. Koroleva[c,m], D. Mondelain[c], G. Piccioni[f], S. Stefani[f], C. L. Strand[g], H. Tran[d], M. Turbet[d,e], A. Vigasin[n], F. Vitali[f], R. Volkamer[i], C. Wei[g]

[a] *NASA Goddard Space Flight Center, Greenbelt, MD, 20771, USA*
[b] *Center for Astrophysics | Harvard & Smithsonian, Atomic and Molecular Physics Division, Cambridge, MA, 02138, USA*
[c] *University of Grenoble Alpes, CNRS, LIPhy, F-38000, Grenoble, France*
[d] *Laboratoire de Météorologie Dynamique/IPSL, CNRS, Sorbonne Université, École normale supérieure, PSL Research University, École polytechnique, F-75005, Paris, France*
[e] *Laboratoire d'astrophysique de Bordeaux, Univ. Bordeaux, CNRS, F-33615, Pessac, France*
[f] *Istituto di Astrofisica e Planetologia Spaziali (IAPS), Rome, 00133, Italy*
[g] *Department of Mechanical Engineering, Stanford, CA, 94305, USA*
[h] *Institute for Atmospheric and Earth System Research/Department of Physics, University of Helsinki, Helsinki, FI-00014, Finland*
[i] *Department of Chemistry & CIRES, University of Colorado Boulder, Boulder, CO, 80309, USA*
[j] *Chemical Sciences Division, National Institute of Standards and Technology, Gaithersburg, MD, 20899, USA*
[k] *Department of Chemistry, Lomonosov Moscow State University, Moscow, 119991, Russia*
[l] *Institut des Sciences Moléculaires d'Orsay (ISMO), CNRS, Université Paris-Saclay, 91405, Orsay-Cedex, France*
[m] *Federal Research Center A.V. Gaponov-Grekhov Institute of Applied Physics, Russian Academy of Sciences, Nizhny Novgorod, 603950, Russia*
[n] *A.M. Obukhov Institute of Atmospheric Physics, Russian Academy of Sciences, Moscow, 119017, Russia*

[*] Corresponding authors:
Email addresses: jacopo.terragni@nasa.gov (J. Terragni), igordon@cfa.harvard.edu (I. E. Gordon)

[o]*Institute of Quantum Physics, Irkutsk National Research Technical University, Irkutsk, 664074, Russia*

Abstract

Collision-Induced Absorption (CIA) phenomena play a key role in the atmospheric energy balance, making their accurate parametrization a decisive factor in modeling planetary atmospheres. This is the primary reason why the HITRAN spectroscopic database includes a dedicated section for CIAs. This section became available for the first time in 2012, followed by its first update in 2019. Five years since the first update, and with a significant amount of new data now available, it is timely to issue a second update. In this update, new data regarding collisional pairs that appear in the CIA section for the first time (H_2–N_2, N_2–Ar, and CO_2–H_2O) are presented. Concerning collisional pairs already present in the database, new data extending both spectral and temperature range are available for CO_2–CO_2, CO_2–H_2, CO_2–CH_4, O_2–O_2, and O_2–CO_2, while new experimental data about H_2–H_2 and H_2–He have been included alongside the respective theoretical calculations. Data sources, comparison among different data, and selection criteria, are discussed in detail. The final section is focused on identifying the CIA data that would be most valuable for the planetary science and astrophysics community in the future.

Keywords:
Collision-induced absorption, HITRAN, Spectroscopic database, Molecular spectroscopy

1. Introduction

Collision-induced absorption (CIA) is a process in which light is absorbed by pairs of molecules due to the dipole moment that is induced by their mutual interaction. The HITRAN database has a specific section that is dedicated to this absorption mechanism. One should note that the CIA is an absorption mechanism in itself, and does not encapsulate the broadening of the monomer absorption lines; however, in the experiments, it is not trivial to distinguish it from the far-wing effect from the strong monomer lines. The CIA section of the HITRAN database was released in 2012 [1], and the

first update was published in 2019 and is presented in the dedicated paper by Karman et al. [2], where CIA-related mechanisms, nomenclature, and general definitions are also presented. This work presents the second update of the CIA section. It is focused on the new data that have been added to the database after a thorough research of the CIA-related works that have been published in the last five years.

The CIA section is organized according to the three main factors that influence this absorption mechanism: 1) the chemical composition of the interacting molecules (*collisional pairs*); 2) the frequency of the absorbed radiation; 3) the temperature of the gas molecules. Consequently, the HITRAN CIA database is organized as follows. Data at various frequency ranges are listed for each collisional pair, and data at various temperatures are available for each frequency range.

CIA data are of great importance in planetary science because CIAs play a crucial role in the thermal balance of planetary atmospheres, influencing the chemical composition and the physical properties of those environments [3]. On Earth, the H_2O-N_2, H_2O-O_2, H_2O-H_2O, and even (to a lesser extent) H_2O-CO_2 collisional pairs contribute significantly to the so-called water continuum [4], which is one of the main drivers of the terrestrial climate [5]. The N_2-N_2 [6, 7, 8], O_2-O_2 [9, 10] (and less dominant N_2-O_2 [8, 11]) also play an important role in modeling terrestrial atmospheric spectra at different wavelengths. On Titan, the warming effect of N_2-N_2 and CH_4-N_2 CIAs inhibits atmospheric condensation on Titan, helping to maintain its dense nitrogen-rich atmosphere [12, 13]. CO_2-CO_2, CO_2-H_2 and CO_2-CH_4 CIAs may be the key to understanding the climate of early Mars and for estimating its past surface temperature [14, 15, 16, 17, 18]. On Venus, multiple CIA bands from CO_2-CO_2 collisions influence how solar radiation is absorbed throughout the various layers of its hot, dense, and CO_2-dominated atmosphere [19, 20]. These examples, beyond underscoring the fundamental role of CIAs in planetary climate modeling, represent atmospheres characterized by very different average temperatures. Consequently, including CIA data at the appropriate temperature range is an important aspect for climate models, and this is why the database lists multiple temperatures for the same frequency range.

However, limiting the relevance of CIAs to atmospheric energy balance alone would be an understatement. For example, (O_2–X) CIAs may represent the most detectable O_2 spectral features in exoplanet transit observations, which can be interpreted as potential biosignatures [21]. In fact, they

may be the only detectable O_2 feature for an Earth-like, cloudy exoplanet atmosphere with biologically produced oxygen when observed by the James Webb Space Telescope (JWST) [22].

Beyond planetary science, CIAs have technological applications as well. They are being explored in the development of compact, responsive, and cost-effective sensors for industrial hydrogen monitoring [23]. In particular, H_2-H_2 and H_2-N_2 CIA processes are promising for accurately detecting hydrogen concentrations during its production, storage, and transportation [24, 23].

The examples above highlight both the broad scientific relevance of CIA and its potential technological impact. From the large list of all the collisional pairs studied so far, the ones included in this publication have been chosen because their binary absorption coefficients have been added to or updated in the HITRAN CIA database. All the database entries that have been inserted/updated discussed in detail in Section 2, where each entry has a dedicated subsection describing the calculation strategy and/or the experimental methodology used to determine the binary absorption coefficients. Section 3 presents a concise discussion of a list of not yet studied collision pairs, frequency ranges, and temperatures which may be important for future investigations in planetary science and astrophysics. Finally, conclusions are reported in Section 4.

2. Data

2.1. General definitions and where to find CIA data

The precise definition of all quantities tabulated in a database is of primary importance, as it eliminates ambiguity and ensures that users can utilize the data correctly. This aspect was discussed in detail in Section 2 of the first update [2], where the data format, the listed quantities along with their corresponding units, and several remarks regarding the distinction between pure gases and mixtures (including air) are presented. Readers are strongly encouraged to consult that section prior to integrating this data into their research activities.

The CIA data can be downloaded from the HITRAN database at `www.hitran.org/cia`. Data are subdivided in two main groups for clarity: *Main* and *Alternate* folder (see Table 1, Column 2). Main contains all recommended data, while Supplementary contains specialized alternatives offering specific advantages (extended temperature ranges, spin statistics incorporation, or line list consistency) that may be useful for particular applica-

tions. Finally, additional information about the data format can be found at www.hitran.org/data/CIA/CIA_Readme.pdf.

2.2. The second update

This second update of the HITRAN CIA section represents a significant enhancement both in terms of collision pairs and absorption bands. Regarding the collision pairs, a total of thirteen have undergone some form of modification, two of which have been included in the database for the first time. As for the absorption bands, several types of changes have been implemented: new bands have been introduced for the first time, some existing data have been replaced with more recent and accurate measurements or calculations, and the temperature range of other bands has been extended. The list of the available bands for each collisional pair is presented in Table 1, where modifications introduced in this second update are highlighted. Moreover, a graphic representation of what is available in the HITRAN CIA database is depicted in Figure 1: this schematic grid displays the collisional pairs for which data are available in the database, along with the kind of absorption bands included (rototranslational, vibrational, or electronic) for each collisional pair.

Of the two collisional pairs that appear in the CIA database for the first time, the first one that is listed in Table 1 is CO_2-H_2O. The CO_2-H_2O CIA has been investigated by Fleurbaey et al. [25] in a study that combines Cavity Ring-Down Spectroscopy and molecular dynamics simulations (see Section 2.13). These new data are extremely relevant for the study of the atmosphere of Early Mars and exoplanets. The second one is N_2-Ar, for which rototranslational and vibrational bands are now available thanks to the computational work of Serov et al. [26], where calculations have been compared with experimental data provided by the same research group [27]. The role of these new CIA in data for modeling nitrogen-rich atmospheres, such as those of Earth or Titan, will be extremely relevant.

This second update also includes data for collisional pairs already present in the database. New data extending both spectral and temperature range are available for N_2-H_2 [23], CO_2-CO_2 [28], CO_2-H_2 [29], CO_2-CH_4 [30, 29], O_2-O_2 [31], and O_2-CO_2 [32], while new experimental data about H_2-H_2 and H_2-He [33] have been included alongside the respective theoretical calculations. Among these data, two bands are listed in the database for the first time: one regards the study of the H_2 fundamental band in H_2-N_2 based on the FTIR spectroscopy experimental work by Wei et al. [23], while the other

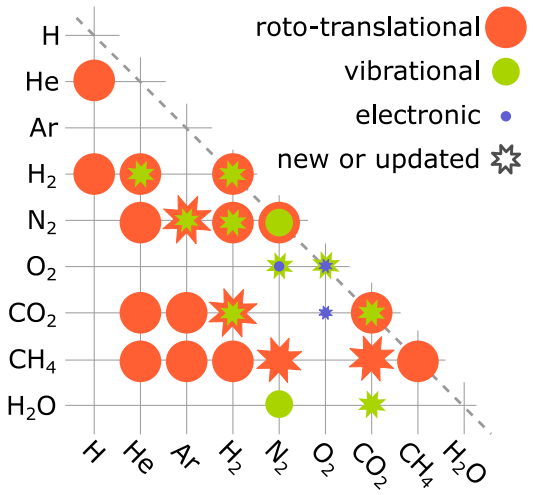

Figure 1: Schematic grid that graphically summarizes which collisional pairs are available in the HITRAN CIA database. The different colors represent the different kind of absorption bands: red for rototranslational, green for vibrational, and blue for electronic. The newly added data are marked with a star-shaped symbol. The diagonal dashed line represents CIA of pure gases.

one regards measurements of the CO_2-CO_2 CIA band around 4000 cm^{-1} performed reported in Tran et al. [28]. Details about these new data, comparison among different data sources, and selection criteria, are discussed in detail in the following subsections.

System	Folder	ν range (cm^{-1})	T range (K)	# of sets	Band description	Reference
H_2-H_2	Main	20-10,000	200-3000	113	Roto-translational, fundamental, 1^{st} overtone	[34]
	Alternate	0-2400	40-400	120	Roto-translational	[35]
	Alternate	2500-6000	120-501	7	Fundamental	[33]
	Alternate	7974-8650	293	1	1^{st} overtone	[36]
H_2-He	Main	20-20,000	200-9900	334	Roto-translational, fundamental, 1^{st}-4^{th} overtone	[37]
	Alternate	2500-6000	121-504	7	H_2 fundamental	[33]

H_2-H	Main	100-10,000	1000-2500	4	Roto-translational, fundamental, 1^{st} overtone	[38]
He-H	Main	50-11,000	1500-10,000	10	Roto-translational	[39]
H_2-CH_4	Main	0-1946	40-400	10	Roto-translational	[40]
N_2-He	Main	1-1000	300	1	Roto-translational	[41]
CO_2-He	Main	0-1000	300	1	Roto-translational	[41]
CO_2-Ar	Main	0-300	200-400	21	Roto-translational	[42]
CH_4-He	Main	1-1000	40-350	10	Roto-translational	[43]
CH_4-Ar	Alternate	1-697	70-296	5	Roto-translational	[12]
CH_4-CH_4	Alternate	0-990	20-800	7	Roto-translational	[44]
CO_2-H_2	Main	5-1500	100-600	6	Roto-translational	[29]
	Alternate	0-2000	200-350	4	Roto-translational	[16]
CO_2-CH_4	Main	0-720	100-600	6	Roto-translational	[30]
	Alternate	5-1200	100-600	6	Roto-translational	[29]
	Alternate	0-2000	200-350	4	Roto-translational	[16]
CO_2-H_2O	Main	5700-6300	296	1	$\nu_3(CO_2) + \nu_1(H_2O)$	[25]
CO_2-CO_2	Main	1-750	200-800	10	Roto-translational	[45]
	Main	1000-1800	200-350	6	Fermi dyad	[46, 47]
	Main	2510-2850	221-297	3	Fermi triad	[47]
	Main	2850-3250	230-298	4	$\nu_2 + \nu_3$ band	[28, 48]
	Main	4000-4500	260-295	2	X band	[28]
N_2-H_2	Main	0-1886	40-400	10	Roto-translational	[49]
	Main	3900-5100	296	1	H_2 fundamental	[23]
N_2-N_2	Main	0-450	70-200	14	Roto-translational	[50]
	Main	0-550	210-300	10	Roto-translational	[50]
	Main	0-650	310-400	10	Roto-translational	[50]
	Main	1850-3000	301-363	5	Fundamental	[51]
	Main	2000-2698	228-272	5	Fundamental	[52]
	Main	4300-5000	200-330	14	1^{st} overtone	[7]
	Alternate	30-300	78-129	4	Roto-translational	[53]
N_2-Ar	Main	0-300	70-500	44	Roto-translational	[26]
	Main	2100-2600	300	1	N_2 fundamental	[26]
	Alternate	2131-2559	300	1	N_2 fundamental	[54]
O_2-O_2	Main	1150-1950	193-353	15	Fundamental	[55]
	Main	7545-8355	246-346	11	$a^1\Delta_g \leftarrow X^3\Sigma_g^-(0,0)$	[56, 57]
	Main	9060-9596	293	1	$a^1\Delta_g \leftarrow X^3\Sigma_g^-(1,0)$	[11]

	Main	10,512-11,228	293	1	$a^1\Delta_g \leftarrow X^3\Sigma_g^-(2,0)$	[58]
	Main	12,600-13,839	296	1	$b^1\Sigma_g^+ \leftarrow X^3\Sigma_g^-(0,0)$	[59]
	Main	14,206-14,898	293	1	$b^1\Sigma_g^+ \leftarrow X^3\Sigma_g^-(1,0)$	[60]
	Main	15,290-16,664	203-287	4	Double transitions*	[61]
	Main	16,644-19,628	203-293	5	Double transitions*	[61]
	Main	20,000-33,670	223-293	3	Double transitions*	[31]
	Alternate	1300-1850	193-356	7	$a^1\Delta_g \leftarrow X^3\Sigma_g^-(0,0)$	[62, 63]
	Alternate	7583-8183	206-346	15	$a^1\Delta_g \leftarrow X^3\Sigma_g^-(0,0)$	[11]
	Alternate	9060-9960	206-346	15	$a^1\Delta_g \leftarrow X^3\Sigma_g^-(1,0)$	[11]
	Alternate	10,535-11,125	206-346	15	$a^1\Delta_g \leftarrow X^3\Sigma_g^-(2,0)$	[11]
	Alternate	12,804-13,402	206-346	15	$b^1\Delta_g^+ \leftarrow X^3\Sigma_g^-(0,0)$	[11]
	Alternate	14,296-14,806	206-346	15	$b^1\Delta_g^+ \leftarrow X^3\Sigma_g^-(1,0)$	[11]
O_2-N_2	Main	1300-1850	193-356	7	O_2 fundamental	[62, 63]
	Main	1850-3000	301-363	5	N_2 fundamental	[51, 64]
	Main	2000-2698	228-272	5	N_2 fundamental	[52, 64]
	Main	7545-8355	246-346	11	$a^1\Delta_g \leftarrow X^3\Sigma_g^-(0,0)$	[56, 57]
	Main	12,600-13,840	296	1	$b^1\Delta_g \leftarrow X^3\Sigma_g^-(0,0)$	[59]
	Alternate	7583-8133	206-346	15	$a^1\Delta_g \leftarrow X^3\Sigma_g^-(0,0)$	[11]
	Alternate	12,804-13,402	206-346	15	$b^1\Delta_g \leftarrow X^3\Sigma_g^-(0,0)$	[11]
N_2-Air	Main	1850-3000	301-363	5	N_2 fundamental	[51, 64]
	Main	2000-2698	228-272	5	N_2 fundamental	[52, 64]
	Main	4300-5000	200-330	14	N_2 1^{st} overtone	[7]
O_2-Air	Main	1300-1850	193-356	7	O_2 fundamental	[62, 63]
	Main	7545-8355	246-346	3	$a^1\Delta_g \leftarrow X^3\Sigma_g^-(0,0)$	[56, 57]
	Main	9091-9596	293	1	$a^1\Delta_g \leftarrow X^3\Sigma_g^-(1,0)$	[11]
	Main	10,512-11,228	293	1	$a^1\Delta_g \leftarrow X^3\Sigma_g^-(2,0)$	[58]
	Main	12,600-13,839	300	1	$b^1\Delta_g^+ \leftarrow X^3\Sigma_g^-(0,0)$	[59]
	Alternate	12,990-13,220	298	1	$b^1\Delta_g^+ \leftarrow X^3\Sigma_g^-(0,0)$	[65]
	Alternate	7583-8183	206-346	15	$a^1\Delta_g \leftarrow X^3\Sigma_g^-(0,0)$	[11]
	Alternate	9060-9960	206-346	15	$a^1\Delta_g \leftarrow X^3\Sigma_g^-(1,0)$	[11]
	Alternate	10,525-11,125	206-346	15	$a^1\Delta_g \leftarrow X^3\Sigma_g^-(2,0)$	[11]
	Alternate	12,804-13,402	206-346	15	$b^1\Delta_g^+ \leftarrow X^3\Sigma_g^-(0,0)$	[11]
	Alternate	14,296-14,806	206-346	15	$b^1\Delta_g^+ \leftarrow X^3\Sigma_g^-(1,0)$	[11]
N_2-H_2O	Main	1930-2830	250-350	11	N_2 fundamental	[66]
N_2-CH_4	Main	0-800	70-400	34	Roto-translational	[67]
	Alternate	0-1379	40-400	10	Roto-translational	[68]

O_2-CO_2	Main	X	X	X	$a^1\Delta_g \leftarrow X^3\Sigma_g^-(1,0)$	[32]
	Main	12,600-13,839	296	1	$b^1\Delta_g^+ \leftarrow X^3\Sigma_g^-(0,0)$	[69]

Table 1: Summary of the different bands for all collisional pairs available in the HITRAN CIA database, both *Main* and *Alternate* folders. The "band description" specifies which (forbidden) monomer transitions the data set corresponds to and, where ambiguous, of which monomer. The newly added entries are highlighted with different colors following the same scheme of Figure 1.

2.3. H_2 – H_2 fundamental band

Main contributors to this section: Francesca Vitali and Giuseppe Piccioni

The fundamental band of H_2 is between 1.5 and 4 μm, a spectral range important, among the others, for the study of the giant planets' atmospheres, where the H_2 CIA represents one of the main sources of their opacity in the IR. Due to the lack of experimental data, new experimental measurements of the H_2-H_2 binary absorption coefficients in the [3600, 5500] cm^{-1} spectral range have been recorded with a Fourier spectrometer coupled with a multi-pass cell inserted in an atmospheric simulation chamber (the experimental setup is described in detail in [70]). The measurements have been performed by Vitali et al. [33] for temperatures from 120 to 501 K and a spectral resolution of 1 cm^{-1}.

Those measurements represent an update of the HITRAN database, where theoretical models [34] have already been added for a wide temperature range. In this spectral region, the colliding molecules go through the $\nu = 1 \leftarrow 0$ vibrational transition and different rotational transitions, generating the Q, S and O lines, which respectively refer to a Δ_J of 0, +2, and -2 (where J represents the rotational quantum number). Those absorption lines are very broad and can't be resolved individually, generating the observed absorption band.

In Figure 2, the H_2-H_2 binary absorption coefficients can be visualized for the seven temperatures investigated.

At room temperature, a comparison of our results with previous experimental data [71, 72, 73, 74] has been made and it is shown in Figure 3.

Good agreement can be observed over the whole band, apart from a deviation of the binary coefficients measured by Brodbeck et al. around 4155 cm^{-1}, where one of the six interference dips is located.

At all the temperatures investigated, the $Q_1(1)$, $Q_1(0)$ and $S_1(1)$ dips have been observed, respectively around 4155 cm^{-1}, 4161 cm^{-1}, and 4713 cm^{-1}.

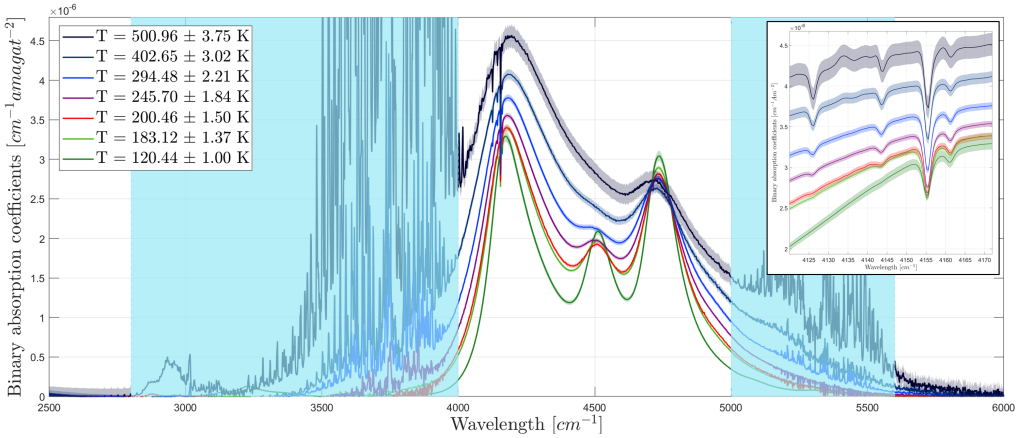

Figure 2: H_2-H_2 binary absorption coefficients for seven temperatures in the [120,501] K temperature range [33]. The light blue shaded regions highlight the spectral ranges where the band was partially affected by water absorption. A blow-up of the four interference dips present on the left side of the main peak of the band is shown in the upper right corner

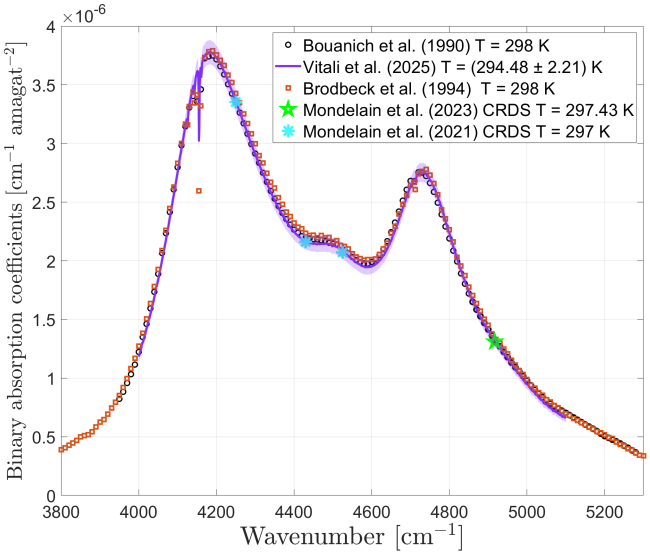

Figure 3: Comparison between our experimental data (solid violet line) and previous works of Bouanich et al. [71] (black circles), Brodbeck et al. [72] (orange squares), Mondelain et al. [73, 74] (green star and light blue asterisks)

The $Q_1(3)$ dip, around 4126 cm^{-1} has been observed for temperatures higher than 200 K, while the $Q_1(2)$ dip around 4143 cm^{-1} has been detected at temperatures higher than 120 K. Finally the $S_1(0)$ dip around 4498 cm^{-1} had been detected just for temperatures below 245 K.
A blow-up of the four dips present on the main peak of the band can be visualized in the upper right corner of Figure 2.
A more detailed study of the dips is a work in progress, thanks to the upgrade of the experimental setup, which will allow us to perform measurements at higher spectral resolution and with all the transfer optics in vacuum. This will drastically limit the amount of water vapor absorption contamination that presently dominates the far wings of the band, as can be seen in Figure 2.

2.4. H_2 – H_2 first overtone around 1.20 µm

Main contributors to this section: A.O. Koroleva and A. Campargue

The binary collision-induced absorption (CIA) of molecular hydrogen has been measured at room temperature in the first overtone region near 1.20 µm [36]. Binary absorption coefficients were derived by cavity ring down spectroscopy (CRDS) at 28 selected spectral points sampling the (2-0) band between 7974 and 8650 cm^{-1}. While all previous studies used high density samples, the sensitivity of the CRDS method allowed deriving accurate CIA by using pressure ramps of pure H_2 limited to a maximum pressure of 1 atm. After subtraction of the Rayleigh contribution, a purely quadratic pressure dependence was obtained for the absorption coefficient at each measurement point and the CIA binary coefficients were derived with a 1.5% accuracy. In Fig. 4, the CRDS results of [36] which are placed in the alternate CIA folder are compared to the theoretical calculations by Abel et al. [34] provided in the main folder. The theoretical values appear to be slightly underestimated by 5-10%. As these differences largely exceed the experimental error bars, the observed deviations give an estimate on the uncertainty of the calculations which have the unique advantage to cover all the frequency range and a large range of temperature values between 200 and 3000 K. The comparison includes also the results of the calculations by Borysow [75] which are also underestimated compared to experiment by a larger amount between 15 and 25% in the considered region. On the experimental side, Brodbeck et al. derived H2-H2 CIA values in the region by extrapolation at zero density of FTS measurements of the H_2 absorption spectrum at densities between 125 and 291 amagat (at 298 K) [76]. The FTS results included in Fig. 4 show an

overestimation by 10-30% compared to the CRDS values [36]. Considering the very long range extrapolation, the achieved level of agreement can be considered as very satisfactory.

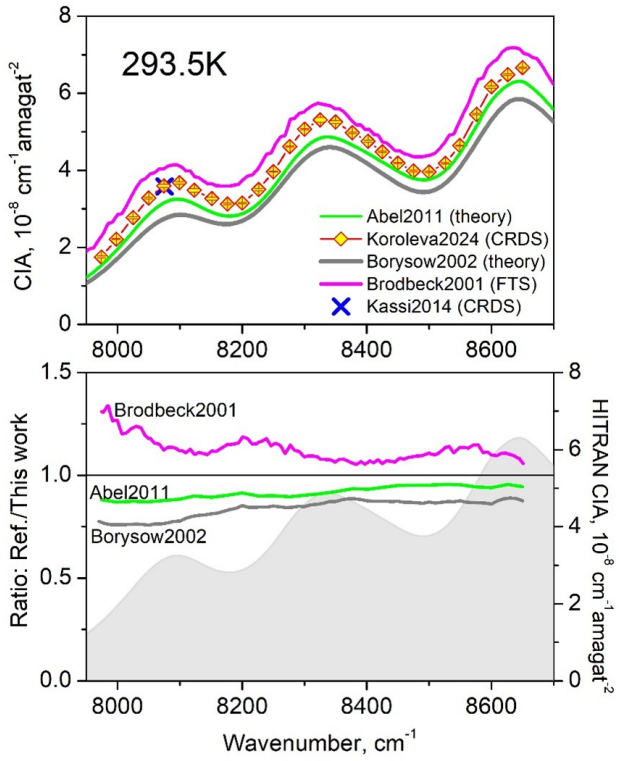

Figure 4: (Adapted from [36]). Frequency dependence of the CIA binary coefficient at 293.5 K in the region of the (2-0) band of H_2 and comparison to previous works. The CRDS measurements of [36] (yellow squares) are compared to calculated values by Abel et al. [34] provided in the CIA main folder of the HITRAN database (grey line) and to calculations by Borysow (green line) [75]. Experimental FTS values by Brodbeck et al. (pink line) were digitized from Fig. 3 of [76]. The CRDS value near 8075 cm^{-1} (blue cross) was obtained from [77].

2.5. H_2 fundamental in H_2 – He and H_2 – N_2

Main contributors to this section: Francesca Vitali and Giuseppe Piccioni for H_2-He, Chuyu Wei and Chris Strand for H_2-N_2

The H_2-He section, which already contained the theoretical models calculated by Abel et al. [37] for temperatures up to 9000 K, have been updated to insert the experimental measurements performed for the fundamental band of H_2 in the [3600, 5500] cm^{-1} spectral range and temperatures from 121 to 504 K [33]. The considered spectral range is important, among others, for the study of the giant planets' atmospheres, where the H_2 CIA represents one of the main sources of their opacity in the IR.
A description of the experimental setup used can be found in [70].
In this spectral region, the absorption band is generated by the broad Q, S, and O lines, which respectively refer to a Δ_J of 0, +2, and -2 (where J represents the rotational quantum number) for the same $\nu = 1 \leftarrow 0$ vibrational transition, generated by the collision between a H_2 molecule and an helium atom.
Figure 5 shows the H_2-He binary absorption coefficients retrieved from the experimental data acquired for the seven temperatures considered.

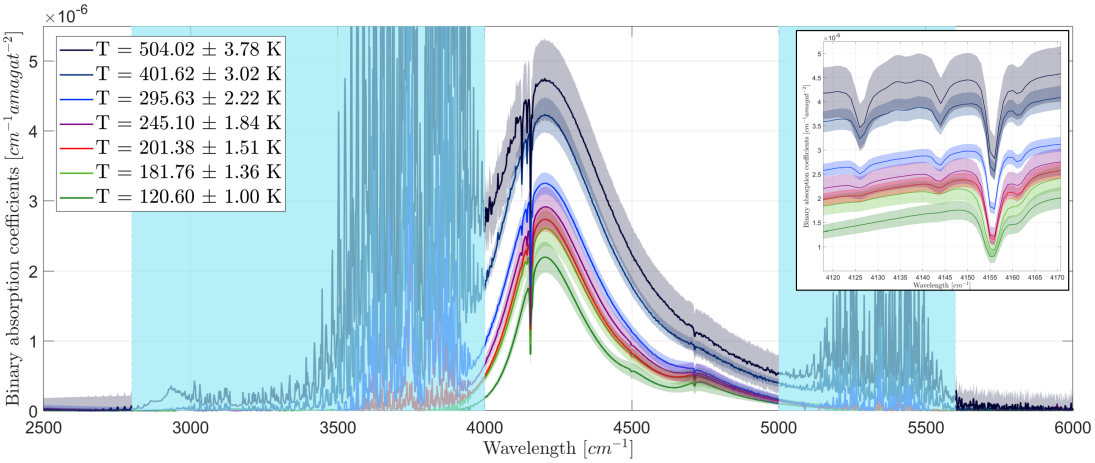

Figure 5: H_2-He binary absorption coefficients for seven temperatures in the [121,504] K temperature range [33]. The light blue shaded regions highlight the spectral ranges where the band was affected by water vapor absorption. A blow-up of the four interference dips present on the left side of the main peak of the band is shown in the upper right corner

At room temperature, a comparison was made between our experimental data and the experimental results obtained by Bouanich et al. [71] and Brodbeck et al. [78] as shown in Figure 6.

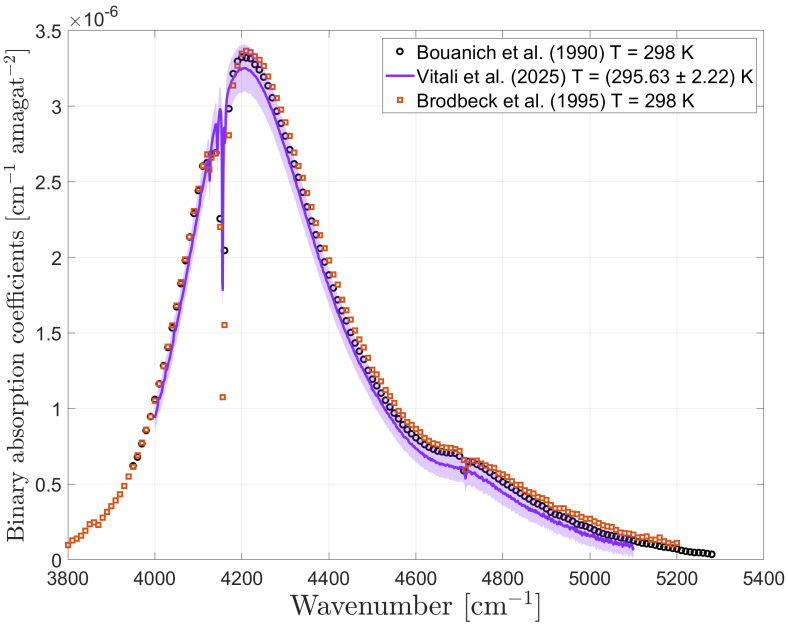

Figure 6: Comparison between our experimental data (solid violet line) and previous works of Bouanich et al. [71] (black circles) and Brodbeck et al. [78] (orange squares)

A good agreement can be noted over the whole band, with a visible deviation of the binary coefficients measured by Brodbeck et al. around 4155 cm^{-1}, where the $Q_1(1)$ interference dip has been observed.
On the H_2-He binary absorption coefficients, the $Q_1(3)$, $Q_1(2)$, $Q_1(1)$, $Q_1(0)$ and $S_1(1)$ dips, respectively around 4126 cm^{-1}, 4143 cm^{-1}, 4155 cm^{-1}, 4161 cm^{-1}, and 4713 cm^{-1}, have been observed at all the temperatures studied, except for the measurement at 120 K, where the $Q_1(3)$ and $Q_1(2)$ are not detected. Moreover, the $S_1(0)$ dip around 4498 cm^{-1} had been observed only for temperatures below 245 K.
A blow-up of the four dips present on the left side of the main peak of the band can be visualized in the upper right corner of Figure 5.
A more detailed study of the dips is a work in progress, thanks to the upgrade of the experimental setup, which will allow us to perform measurements at higher spectral resolution and with all the transfer optics in vacuum.
This will drastically limit the amount of water vapor absorption contamination that presently dominates the far wings of the band, as can be seen

in Figure 2. We also plan to investigate the dependence of the dips on the helium concentration.

New experimental measurements of the H_2-N_2 binary absorption coefficients in the H_2 fundamental band, reported by Wei et al.[23], have been added to the main folder for the first time. These measurements were conducted at room temperature over a pressure range of 0 – 61 atm using a FTIR spectrometer with a resolution of 0.5 cm^{-1}, coupled with a 29.12cm high-pressure optical cell. The binary absorption coefficients of the H_2-N_2 pair were inferred using measurements of a 20% H_2/80% N_2 mixture by subtracting H_2-H_2 contribution based on pure H_2 measurements. The resulting coefficients are presented in Fig. 7 and compared with the earlier data by Hunt and Welsh [79]. While the measured H_2-H_2 binary absorption coefficients from Wei et al. generally agree with those of Hunt and Welsh, the CIA cross sections for the H_2-N_2 pair near the intercollisional dip differ by approximately 40%. It is worth noting that the H_2-N_2 binary coefficients reported by Hunt and Welsh were obtained using H_2/N_2 mixtures up to 300 atm, whereas the H_2-H_2 measurements were limited to pressures up to 100 atm. Therefore, the observed discrepancies in the H_2-N_2 data are likely due to higher-order effects at elevated pressures. The values reported by Wei et al., derived under more moderate and binary-representative conditions, are considered more accurate for binary absorption and have been included in this update. These measurements were further validated across different H_2/N_2 mixture ratios and showed good agreement. Additional details regarding the experimental setup and validation procedures can be found in Ref. [23].

2.6. N_2 – Ar roto-translational band

Main contributor to this section: E.A. Serov + collaborator(s). Waiting for data.

Argon is a significant component in planetary atmospheres, and although its abundance is usually relatively low, the N_2-Ar CIA spectra may still be relevant in modeling nitrogen-rich atmospheres. Furthermore, it is speculated that N_2-X CIA data at elevated temperatures could be of importance for characterizing the cold stars' atmospheres. However, the current dataset is limited to temperatures up to 500 K, and future studies will be necessary to extend this range to higher temperatures.

The N_2-Ar CIA coefficients are introduced for the first time, based on the data issued from the trajectory-based simulations carried out in Ref. [26].

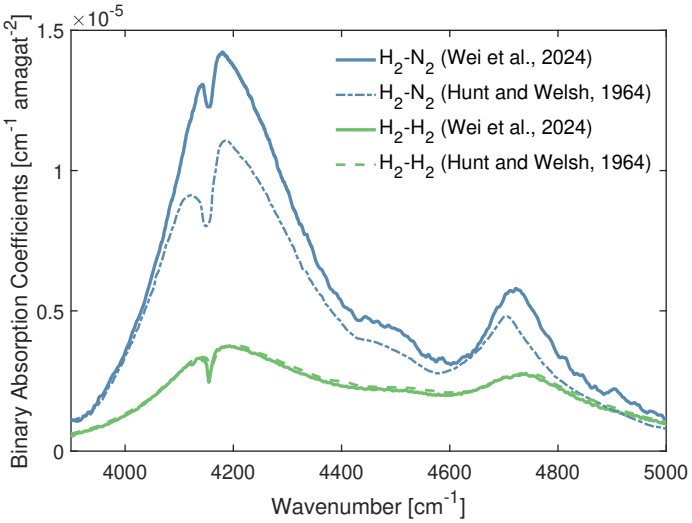

Figure 7: Comparison between the measured H_2-N_2 CIA absorption coefficients by Wei et al. (solid lines), now included in HITRAN, and earlier data by Hunt and Welsh (dash lines), both at room temperature.

The simulation of N_2-Ar CIA opacity was conducted using the trajectory-based approach extended to include the vibrational mode of N_2, allowing to assess the validity of the conventionally used approximation of rigid monomers. To achieve this, the full-dimensional representation of the two-body components of the intermolecular energy and induced dipole was constructed by applying the permutationally-invariant polynomial neural-network (PIP-NN) approach, which is discussed in detail in application to weakly bound systems in Ref. [80]. During the construction of the surfaces, the range of variation of the N_2 bond was chosen to enable the description of monomer vibrational excitations up to 3,000 cm^{-1}. Ab initio values for both intermolecular energies and induced dipoles were derived quantum-chemically at dense grids using the coupled-cluster level of theory. The contributions from both bound and unbound states were accounted for using the same computational scheme.

HITRAN CIA tabulates 44 spectra for temperatures spanning from 70 to 500 K. To simulate the N_2-Ar rototranslational band at each temperature, an ensemble of 2 million trajectories was employed, and Schofield's desymmetrization procedure was applied to bring it in correspondence with the quantum detailed balance principle. As shown in Figure 8, the results of the trajectory-based simulation exhibit satisfactory agreement with the

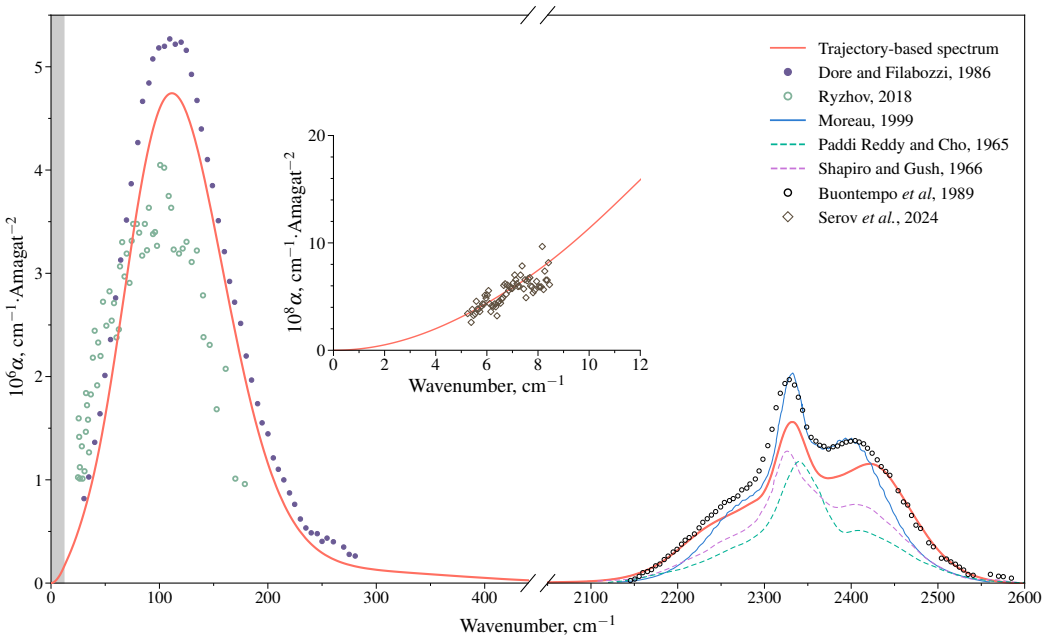

Figure 8: N_2-Ar collision-induced absorption spectra at 300 K in the rototranslational band and the N_2 fundamental. The red curve represents the results of the trajectory-based simulation reported in Ref. [26], which are compared to available experimental data: Refs. [81, 82, 26] in the RT band and from Refs. [54, 83, 84, 85] in the N_2 fundamental. A shaded area highlights a frequency range that is shown in the inset, where a trajectory-based result is compared to subTHz measurements from Ref. [26].

measurements reported by Dore and Filabozzi [81] and Ryzhov [82].

In Ref. [26], millimeter-wave spectra of the N_2-Ar mixture were recorded using a resonator spectrometer [27] over a temperature range of 278–333 K and a frequency range of 170–260 GHz. A comparison with these measurements, displayed in the inset of Figure 8, revealed a discrepancy with the trajectory-based result of less than 5%.

2.7. N_2 fundamental in N_2 – Ar

Main contributor to this section: E.A. Serov + collaborator(s). Waiting for data.

We include N_2-Ar CIA coefficients at 300 K in the N_2 fundamental based on the theoretical results from Serov et al. [26], which spans from 2,100 to 2,600 cm^{-1}. As outlined in preceding section, the trajectory-based framework was extended to accommodate the N_2 vibration [26], enabling for simultaneous modeling of CIA in both the rototranslational band and the N_2 fundamental band. To achieve converged spectral profile, an array of 60 million classical trajectories was employed. Due to the stiffness of the N_2 vibrational mode, it remains largely inactivated when a classical trajectories examination is performed at temperatures in the 70–400 K range. And thus only the harmonic variation in the potential energy determines the resulting position of the CIA band. To address this, the theoretical spectrum's band center, as presented in Figure 8 and in HITRAN tables, has been shifted to align with the observed band's maximum at 2392.92 cm^{-1}. Additionally, a combination of two quantum corrections was applied to the classically calculated N_2-Ar CIA band in N_2 fundamental. First, a procedure put forward by Bader and Berne [86], which is commonly employed for adjusting vibrational IR amplitudes, was utilized assuming absolute frequency scale. Second, the profile was subject to procedure due to Schofield [87] with the frequency determined in relation to the band center. The trajectory-based profile is shown in Figure 8, alongside a set of experimental data from Refs. [54, 83, 84, 85]. Additionally, the CIA coefficients measured by Moreau [54] are provided in the Alternate folder for reference.

2.8. CH_4 – N_2

Main contributors to this section: Artem Finenko + Iouli Gordon

In exoplanet studies, nitrogen-dominated atmospheres are explored for super-Earths [88, 89]. Particularly in regimes analogous to that of warm Titan it is likely that the radiative balance is influenced by the CH_4-N_2 CIA. A

prominent example of a nitrogen-based atmosphere in Solar System is Titan, where CH_4-N_2 CIA is the prevailing source of opacity in the 150–450 cm^{-1} region. In the Richard et al. [1] effort, data for CH_4-N_2 CIA, determined by Borysow and Tang [68], was adopted. The Main Folder CH_4-N_2 is now updated with the results of the trajectory-based consideration conducted in Finenko et al. [67], which provides data at 34 temperatures ranging from 70 to 400 K.

Within the trajectory-based approach, while treating collision partners as rigid rotors, the time-evolution of interaction-induced dipole is accumulated over an ensemble of 5-10 million classical trajectories. The resulting dipole correlation function is subsequently transformed into a CIA spectrum via a Fourier transform. The utilized intermolecular potential and induced dipole surfaces were obtained from the Ref. [90], were they were constructed based on the *ab initio* data calculated at the coupled-cluster level of theory. The classically derived trajectory-based profiles were subject to desymmetrization procedure, which involved a linear combination of the desymmetrization factors put forward by Schofield [87] and Frommhold [91]. This semi-empirical CH_4-N_2 CIA model was incorporated in the radiative transfer model of Titan's atmosphere of Bézard and Vinatier [92] to generate synthetic radiance spectra. The parameters of the linear-weighted desymmetrization were optimized to reproduce the radiance measurements performed by the Composite Infrared Spectrometer (CIRS) [93] aboard the Cassini spacecraft. As shown in Figure 9, synthetic profiles simulated using the semi-empirical CH_4-N_2 CIA model exhibit excellent agreement with the CIRS data. Simulations using the Borysow and Tang's CH_4-N_2 CIA data resulted in poorer agreement with the CIRS measurements, which has led to proposals for introducing heuristic correction factors to improve modeling accuracy [94, 92].

The opacities calculated by Borysow and Tang [68] are based on effective isotropic potentials combined with adjusted short-range induced dipoles, for which the intrinsic parameters were derived by fitting to experimental spectra. However, since the experimental data are only available down to 126 K [95], it is not surprising that differences are observed between the semi-empirical data of Finenko et al. [67] and Borysow and Tang's data [68] for temperatures in the 70–100 K range, which is primarily targeted by the CIRS/Cassini measurements.

The trajectory-based results agree closely with the available experimental data [95, 96, 97], as illustrated in Figure 10, which compares the theoretical data with measurements from Birnbaum et al. [96] at two representative

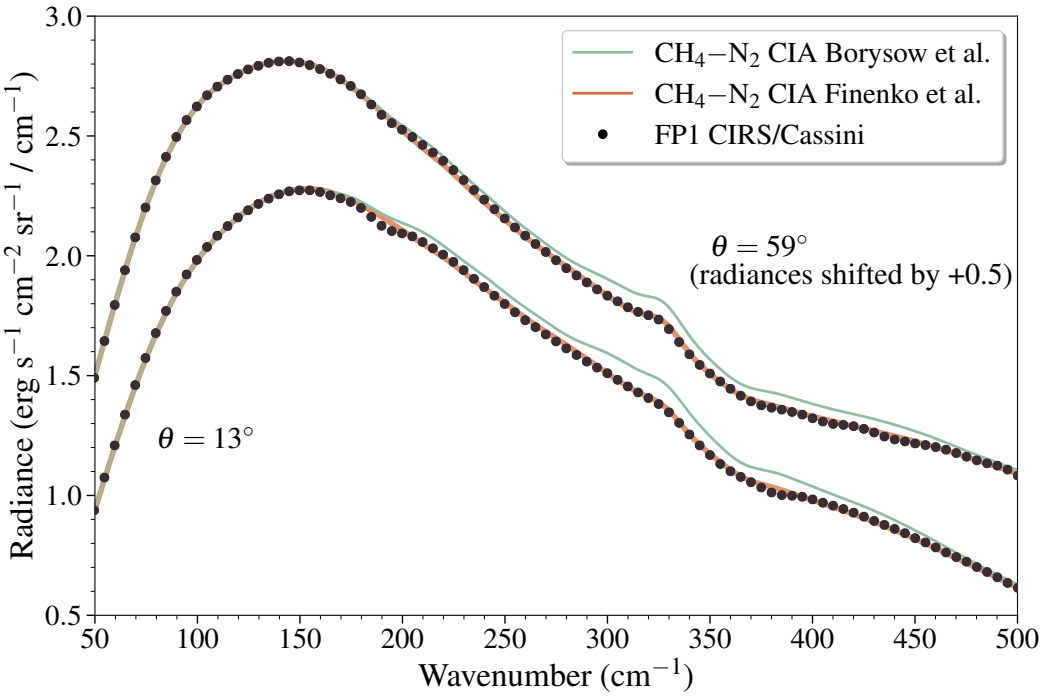

Figure 9: Far-infrared Titan's emission spectra at low (13°) and high (59°) angles. Synthetic spectra simulated using the CH_4-N_2 CIA of Borysow and Tang [68] and the trajectory-based data of Finenko et al. [67] are shown as green and orange lines, respectively. The Cassini/CIRS measurements are represented by solid black circles. For clarity, the high-angle emission spectra is shifted by 0.5 erg s^{-1} cm^{-2} sr^{-1} / cm^{-1}.

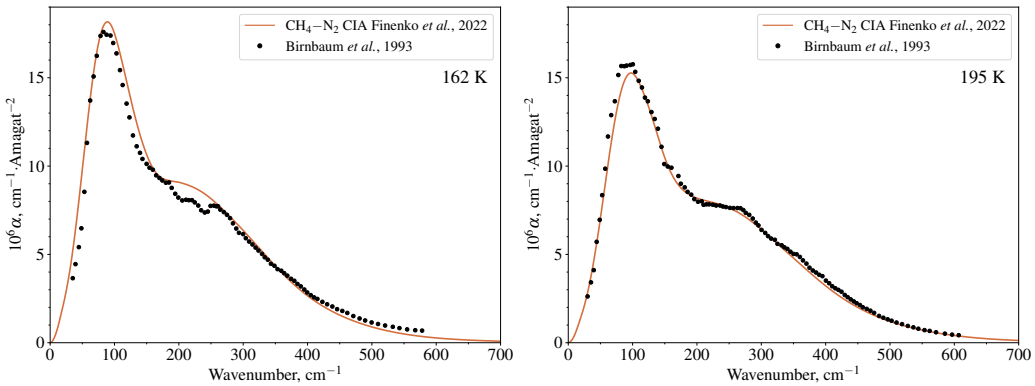

Figure 10: CH_4-N_2 collision-induced absorption spectra at 162 K and 195 K. Theoretical results from Finenko et al. [67] are represented with orange lines, while experimental measurements from Birnbaum et al. [96] are denoted with solid circles.

temperatures. Recent experimental measurements of CH_4-N_2 CIA reported by Johnson et al. [97] in the 30–400 cm^{-1} range at approximately 130 K provide validation for Finenko et al.'s data [67]. The positions of primary and secondary absorption peaks in the measurements [97], which are 75 and 206.5 cm^{-1}, and are in close agreement with those of Finenko et al.'s data [67], which are 80 and 206 cm^{-1}. However, the data of Borysow and Tang [68] exhibit a secondary peak at 158 cm^{-1}, which is notably different from the experimentally measured position.

2.9. CO_2 – CO_2 ($\nu_1/2\nu_2$) around 7.5 µm

This section is blocked for now as there are still data that need to be processed. Main contributors to this section: Jacopo Terragni, Erika Kohler, H. Tran, J.-M. Hartmann

The HITRAN CIA section has been interested by multiple changes regarding the CO2-CO2 collisional pair in this second update. In particular, the Fermi dyad region (1100 - 1800 cm-1) has been updated with new data covering a large range across room temperature, which now span from 192 K to 500K.

The first subset of Fermi dyad data covers the temperature range from 192 K to 360 K. These experimental data refer to the work of Baranov et al. (2004) [55] and have been recently recovered. These newly recovered data expand both the temperature range and the number of temperatures

Figure 11: The different CO_2-CO_2 CIA bands available in the HITRAN database.

for which binary absorption coefficients are listed with respect to the previous update [2].

The second subset of Fermi dyad data consists of the recent experimental data reported by Terragni et al, [**?**]. In this work, a series of CO_2 spectra were collected from 300 K to 500 K (25 K steps) and a resolution of 0.5 cm^{-1}. Measurements were performed integrating a SPECAC environmental cell (3 cm path lenght) into a Bruker Invenio R FTIR spectrometer. Details about the experimental apparatus, measurement procedure, and data analysis are reported in [**?**] with particular emphasis on the technical aspects implemented to avoid water contamination. The Fermi dyad is a CO_2-CO_2 CIA band showing a characteristic true dimer absorption superimposed to a smooth feature resulting from free-free collisions and quasi-bound pairs [**?**]. Gas cells with long path lengths (tens of meters) are generally used for CIA measurements [46, 48, 28], while the one of the environmental cell used in [**?**] is considerably shorter, requiring a much higher gas number density. Consequently, the true dimer absorption features are not resolved due to pressure broadening. To overcome this, spectra are fitted using the Fermi dyad band shape proposed by Tran et al. [28] in which true dimer features are included. This semi-empirical model is based on the Baranov et al. [55] dataset and is valid up to 500 K. A selection of the new data for the Fermi dyad is reported in Figure 11.

2.10. CO_2 – CO_2 3(ν_1/2ν_2) around 4000 cm^{-1}

Main contributor to this section: H. Tran and J.-M. Hartmann

Absorption of pure CO_2 in the 4000-4500 cm-1 region were recorded at 295 K and 260 K, for pressure up to 40 bars, using a Fourier transform spectrometer with a resolution of 1 cm^{-1} and a single-pass cell of 215 cm. Three CIA bands were observed at 4060, 4277, and 4380 cm^{-1}, with the most intense band located at 4060 cm^{-1}. For this band, the measured binary absorption coefficients yield band-integrated intensities of (4.10 ± 0.65) $10^{-6} cm^{-1} amagat^{-2}$ at 295 K and (5.03 ± 3.08) $10^{-6} cm^{-1} amagat^{-2}$ at 260 K. The much larger uncertainty at 260 K is due to the higher noise level of the spectra measured at this temperature. The measured band-integrated intensities and band shapes are in good agreement with values previously

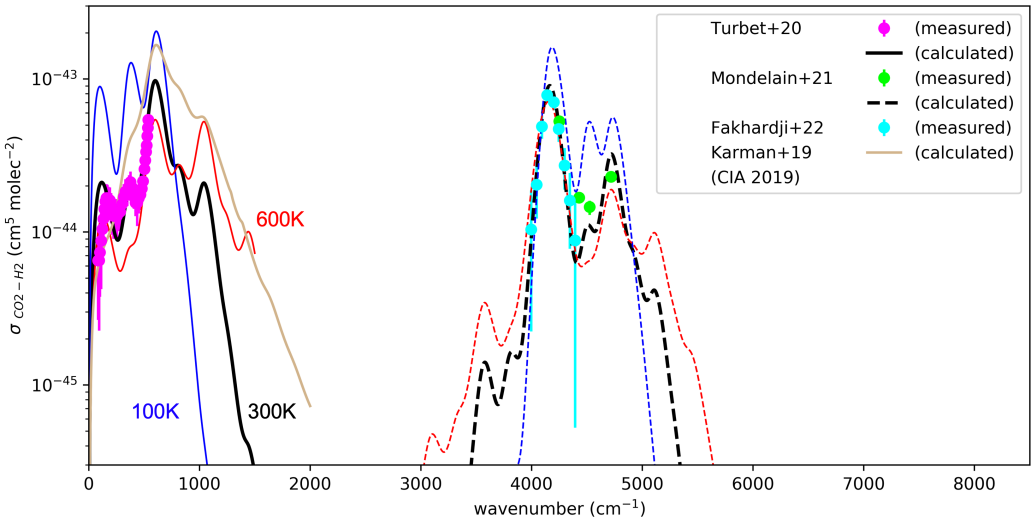

Figure 12: CO_2-H_2 collision-induced absorption spectra at 300K, along with model predictions at 100 and 600K [29, 73]. Theoretical results from refs. [29] and [73] are represented with black solid and dashed lines, respectively. Experimental measurements from refs. [29], [73] and [99] are denoted by magenta, lime and cyan colors, respectively. Previous data from HITRAN CIA 2019 (ref. [2] ; shown for comparison), based on theoretical calculations from ref. [16], is represented by the grey line.

reported in Ref. [98]. Finally, note that due to the high pressures considered, the large spectral resolution, and the low signal-to-noise ratios, no clear dimer signatures were observed for these CIA bands.

2.11. CO_2 – H_2

Main contributor to this section: Martin Turbet and Didier Mondelain

The CO_2-H_2 CIA is a source of absorption that has been proposed as the potential greenhouse contribution responsible for the increase of the surface temperature of a CO_2-dominated early Martian atmosphere above the melting point of water [15, 16, 18]. This could potentially explain the presence of aqueous mineralogic and geomorphologic features visible today on the ancient terrains of Mars [100]. In this update, the binary coefficients in the main folder correspond to the output of the semi-empirical model detailed in Appendix A of [29] and in [73]. These calculations are based on the "isotropic approximation" and provide the area-normalized spectral shape of

the CIAs. The latter are then multiplied by the integrated intensity calculated using the formalism developed by Gruszka and Borysow [101] to fully account for the influence of the intermolecular potential anisotropy on the 0th order spectral moment of the band. This model has the advantage of providing data over a large range of wavenumber and temperature. Here data are given in the 0–1500 and 2500–6000 cm^{-1} spectral regions for temperatures spanning between 100 to 600 K. Three sets of experimental data have been used to test/validate this model at room temperature. A first one covering the 50–550 cm^{-1} interval comes from spectra recorded for various mixtures of CO_2 and H_2 with the Bruker IFS 125HR Fourier transform spectrometer (FTS) of the AILES line at the SOLEIL synchrotron. The experimental setup as well as the spectra treatment are described in [102]. The measured CO_2-H_2 CIA is presented in [102], and updated in [29] with significantly lowered uncertainties, thanks to a second measurement campaign where the stability of the helium-cooled detector temperature was improved. The second dataset was also obtained using the AILES line at the SOLEIL synchrotron, but cover the 3950-4350 cm^{-1} interval, thanks to a change in the experimental design permitted by the implementation of diamond windows [99]. The third dataset is derived from absorption spectra obtained with a cavity ring down spectrometer (CRDS) in Grenoble for four spectral intervals in the 4255–4720 cm^{-1} CO_2 transparency window which is within the (1-0) band of H_2. Series of spectra were recorded for two mixtures of H_2 + CO_2 with different fractions of H_2 (∼70% and ∼30%) and at different pressures between 10 and 93 kPa.

Binary coefficients calculated at 300 K are in reasonable agreement with the experimental data for the roto-translational band [29] and the central part of the region of the fundamental band of H_2 [99], but some discrepancies remain (see Fig. 12) certainly due to the isotropic approximation for the interaction potential and to the fact that the short range components of the induced dipole is neglected.

The binary coefficients calculated in [16] are provided in the alternate folder for the 0-2000 cm^{-1} spectral range and for temperatures between 200 and 350 K. In this latter work, the CO_2-H_2 CIA is calculated from a linear combination of the known H_2-H_2 and CO_2-CO_2 CIAs with the spectrally integrated intensities of these new CIAs determined from ab initio calculations of the zeroth order spectral moment. Comparison of these calculated values to the experimental data and to the data provided in the main folder are plotted in Figs. 1 and 2 of [29] and shows a quite large overestimation of the

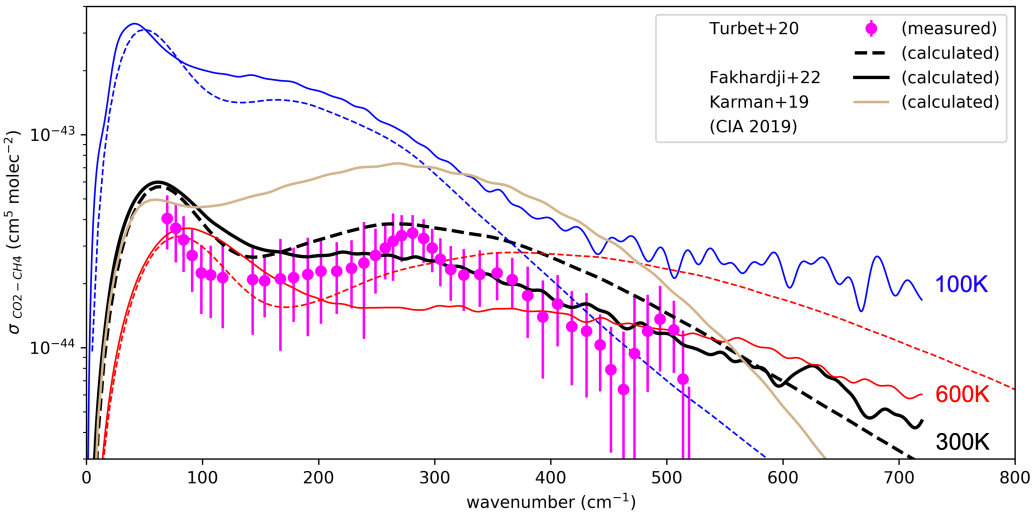

Figure 13: CO_2−CH_4 collision-induced absorption spectra at 300K, along with model predictions at 100 and 600K [29]. Theoretical results from refs. [30] and [29] are represented with black solid and dashed lines, respectively. Experimental measurements from ref. [29] are denoted by magenta color. Previous data from HITRAN CIA 2019 (ref. [2]; shown for comparison), based on theoretical calculations from ref. [16], is represented by the grey line.

absorption for the former dataset.

2.12. CO_2 – CH_4

Main contributors to this section: J.-M. Hartmann and Martin Turbet

A consistent number of works have been dedicated to the CO_2-CH_4 collisional pair in the last few years, all of them motivated by the fact that CH4 could have been an effective warming agent in the reducing atmosphere of early Mars [15, 16, 18]. The HITRAN CIA section has been updated with two new entries.

The first one regards the data reported in Fakhardji et al. [30] and has been made available in the Main folder. In [30] the far-infrared (roto-translational) CIA of CO_2-CH_4 mixtures was computed using classical molecular dynamics simulations. The rotational and translational dynamics of the molecules were computed using the CO_2-CH_4 intermolecular potential proposed by Hellmann et al. [103], along with the long-range development of the interaction-induced dipole provided by Li et al. [104] (see Eqs. (1)-(3) therein), fed by the numerical values provided in Table IV of the same work.

This enables the prediction of the induced dipole autocorrelation function which, after introducing a *desymmetrization* factor and performing a Fourier transform, provides the absorption spectrum. The effect of different desymmetrization procedures (see Eqs. (6)-(9) in [30]) is presented in detail and compared with the so-called "isotropic approximation", showing how this latter procedure leads to CIA underestimation. Calculations using different desymmetrizations are compared with experimental measurements (at room temperature) reported in [29]. Due to the satisfactory agreement between predictions obtained by using the "P2" desymmetrization and experimental data (see Fig. 13), P2-based results have been included in this HITRAN CIA update for temperatures of 100, 200, 300, 400, 500 and 600 K.

The second set of data can be found in the Alternate folder and refers to the semi-empirical calculations reported in Turbet et al. [29] which provide CIA binary absorption coefficients across a broad spectral domain (0-1500 cm^{-1}) and for a wide range of temperatures (100–600 K). This model is grounded on experimental measurements recorded at the AILES line at the SOLEIL synchrotron facility [102, 29], using a Bruker IFS 125HR Fourier transform spectrometer (FTS) and a 2.5 m long multi-pass cell (see Section 2.1 of [102] for additional details on the experimental apparatus). The model is based on the "effective" isotropic potential proposed by Bastien et al. [105] and the empirical short-range components of the induced dipole are included following the approach of Borysow & Tang [106]. Additional details about this model can be found in the supplementary material of [29].

2.13. CO_2 – H_2O

Main contributors to this section: H. Fleurbaey and A. Campargue

The continuum in $H_2O - CO_2$ mixtures is important for the Venusian atmosphere [107, 19] and potentially for the atmospheres of Early Mars [108], early Earth and exoplanets [109]. In addition to the far wings of the CO_2 and H_2O resonance lines broadened by collisions with H_2O [66, 110, 111, 112] and with CO_2 [110, 113, 112], respectively, a CIA band has been measured near 6000 cm^{-1}. This band has been observed in spectra of humidified CO_2 recorded by cavity ring down spectroscopy (CRDS) at pressures below atmosphere [25]. It corresponds to the simultaneous excitation of $^{12}CO_2$ and H_2O colliding molecules in the ν_3 antisymmetric and ν_1 symmetric stretching mode, respectively. This attribution is validated by (i) the good agreement with classical molecular dynamics simulations (CMDS) of the considered CIA

based on the dominant dipole induction mechanism associated with the vibrational matrix elements of the dipole of CO_2 (ν_3) and isotropic polarizability of H_2O (ν_1) and (ii) the CRDS spectra recorded near 5940 cm^{-1} with a highly enriched $^{13}CO_2$ sample since the measured CIA isotopic spectral shift ($\sim$ -68 cm^{-1}) coincides with that between the ν_3 bands of $^{12}CO_2$ and $^{13}CO_2$. The binary coefficients (in $cm^{-1}amagat^{-2}$) are provided here between 5700 and 6300 cm^{-1} from a Lorentzian function with the experimental parameters reported in Table 1 of [25] for the $\nu_3(^{12}CO_2) + \nu_1(H_2O)$ CIA band.

2.14. O_2 – O_2, O_2 – N_2 and O_2 – air $^1\Delta$ band

Main contributors to this section: Erin Adkins and Didier Mondelain

The weak $^1\Delta$ band near 1.27 μm is increasingly called upon for air-mass determination from ground-based and space-borne atmospheric spectra because of its spectral proximity to CO_2, and CH_4 bands at 1.6 μm, in contrast to the more distant A-band at 0.76 μm. For this purpose, it is important to well characterize not only the narrow absorption lines but also the strong underlying broad CIA structure and its temperature dependence. This latter has been experimentally characterized in works of Refs [114] and [56] at 296 K and in Ref. [57] at 271 and 332 K. This lead to the measurement of the B_{O2-O2}, B_{O2-N2} and B_{O2-air} binary coefficients for the $O_2 - O_2$, $O_2 - N_2$ and $O_2 - air$ systems, respectively. Compared to the HITRAN2020 version, in this updated version the data of Maté *et al.* [115] are replaced in the main folder by the ones derived from Refs. [56] and [57]. More precisely, data provided here correspond to the binary coefficients (in $10^{-6}cm^{-1}amagat^{-2}$) of the CIA, and their uncertainties, for the B_{O2-O2}, B_{O2-N2} and B_{O2-air} binary coefficients from 246 to 346 K with a temperature step of 10 K in the 7545 - 8355 cm^{-1} range. The adopted spectral step is 1 cm^{-1}. These coefficients (Figure 14) are derived from the measurements done at 271, 297 and 332 K by CRDS and described in Refs. [56] and [57]. The binary coefficients at the temperature T for a given system $O_2 - x$ are derived using Eq. 1 and the $B_{O_2-x}(297K)$ and $\frac{dB_{O_2-x}}{dT}$ values of [57].

$$B_{O_2-x}(T) = B_{O_2-x}(297K) + \frac{dB_{O_2-x}}{dT}(T - 297K) \quad (1)$$

The uncertainties of the binary coefficients are calculated from the estimated uncertainties on the binary coefficient at 297 K, $UncB_{O_2-x}(297K)$, and on the temperature dependence coefficient, $Unc\frac{dB_{O_2-x}}{dT}$ [57] with:

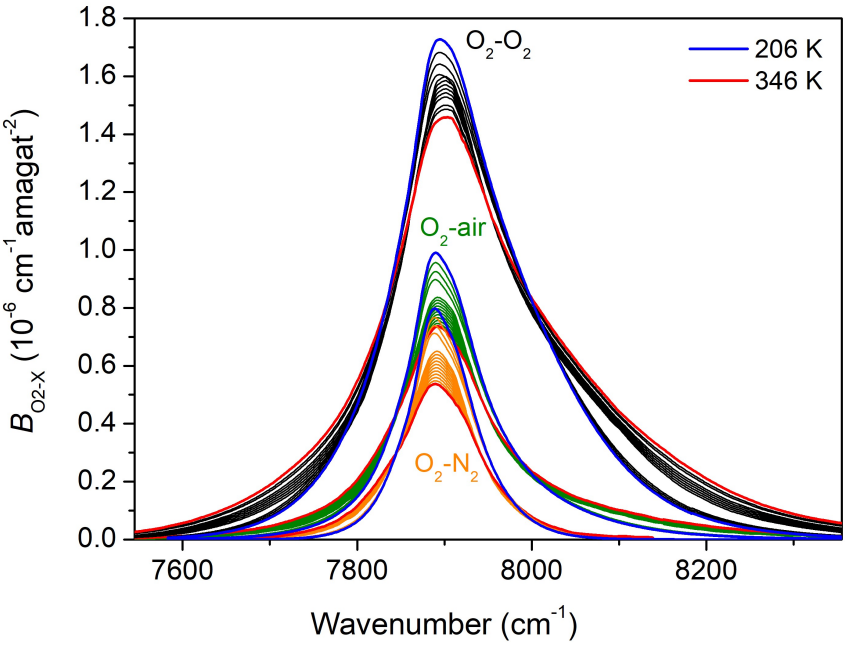

Figure 14: Overview of the binary coefficients provided in HITRAN2024 for the singlet delta band between 206 and 346 K.

$$UncB_{O_2-x}(T) = UncB_{O_2-x}(297K) + Unc\frac{dB_{O_2-x}}{dT}abs(T - 297K) \quad (2)$$

To extrapolate the temperature range of the binary coefficients down to 206 K, the parametrized model of recent quantum calculations for CIA [11], which is detailed in [116], is applied between 206 and 236 K. In this parameterized model, B_{O2-O2} and B_{O2-N2} are given by the superposition of the spin-orbit and exchange mechanism line shapes reported by Karman et al. [11] scaled by temperature-dependent mechanism intensities, which were adjusted to simultaneously model the previously described CRDS measurements of B_{O2-O2}, B_{O2-N2} and B_{O2-air} at various temperatures [114][56][57]. Systematic differences between the parameterized CIA model and measurements result in integrated binary absorption coefficients that differ by less than 2.7 % over the measured temperature range [116]. While this shows good agreement between measurements and theory, recent measurements report O_2-air integrated binary absorption coefficient differences of only 0.11% [114]. The difference between the parameterized model and measurements justifies the CRDS measurements described above being used in HITRAN2024 in the temperature ranges where they can be extrapolated with confidence (246 K – 346 K)[56][57] and using the parameterized model beyond that region (206 K – 236 K) [116]. The uncertainties of the binary coefficients given by the parameterized model are defined as the mean of the maximum magnitude differences between the parameterized model and the binary coefficients given by Eq. 1 over the temperature range where the parameterized model was optimized.

2.15. O_2 – O_2 Double transitions

Main contributors to this section: H. Finkenzeller and R. Volkamer

The double transitions in the UV-VIS spectral range are important for the detection of several gases that have overlapping absorption features in this wavelength range, e.g., BrO, HCHO, NO_2, CHOCHO.

The data for the double transitions in the range $20\,000 - 29\,800\,cm^{-1}$ were updated, the data in the range $29\,800 - 33\,670\,cm^{-1}$ were added. The source study, using a cavity enhanced absorption spectrometer similar to the study underlying the previous data[61], but employing an optimized data acquisition and analysis approach, accomplished to spectrally resolve the relatively weak transitions at 315, 328, 428, 495 nm. The absorption at 495 nm

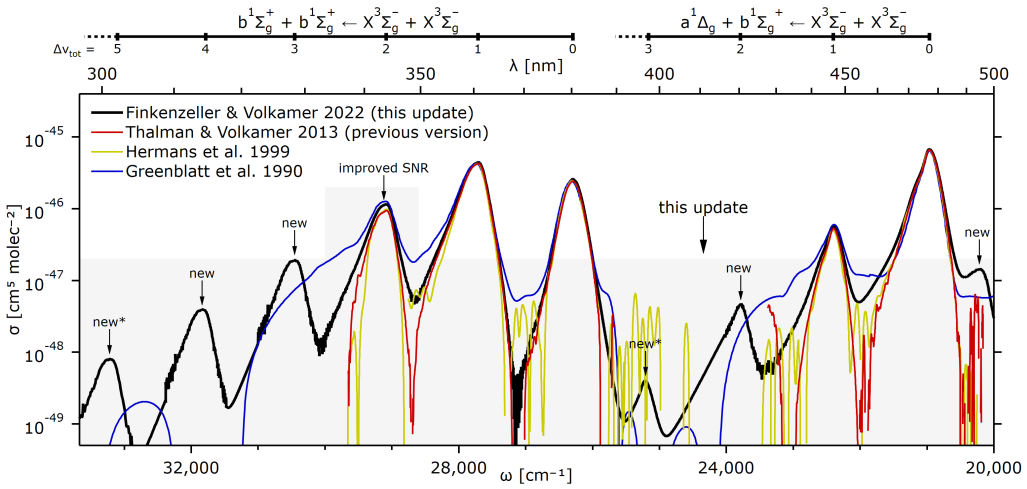

Figure 15: Update to the O_2 – O_2 double transition cross section in the 20 000 – 29 800 cm^{-1} range (293 K) and comparison to previous data.[31, 61, 117, 118] The weak transitions labeled with an asterisk (303 and 397 nm) are not measured but extrapolated from the trend in each system. Note the non-zero absorption for the entire spectral range, resulting from the instrument baseline correction assuming exponentially decreasing absorption in the wings of transitions.

corresponds to the transition $a^1\Delta_g + a^1\Delta_g \leftarrow X^3\Sigma_g^- + X^3\Sigma_g^-$, $\Delta\nu_{\text{tot}} = 3$. The absorption at 340 nm is determined with a higher signal to noise ratio, resulting in different shape and intensity. The accounting for the instrument baseline does not make the assumption of zero absorption between bands [117, 61], but uses exponentially decreasing absorption in the wings of the transitions. The trend within the systems was used to extrapolate the even weaker transitions at 303 and 397 nm.[119] As a result of the baseline correction and extrapolation of transitions, the continuum CIA in the range of 20 000 – 33 670 cm^{-1} is estimated. The integral cross section (of the transitions with sufficient SNR) is found to increase slightly with temperature (223, 263, 293 K).[31]

The updated cross section has been found to significantly improve the fit quality and reduce the uncertainties for retrievals in the UV spectral range.[120] The previously observed but unmeasured absorption at 328 and 428 nm [121] is now resolved. The accuracy of the cross section regarding temperature was demonstrated in an atmospheric field study.[10] Since its publication in 2022, the new data have been used in the retrieval of e.g.

BrO[122], IO[123], HCHO[124, 125], CHOCHO[126], NO_2[120], H_2O[127].

An increasing number of studies confirm that the cross section is quantitatively accurate for remote sensing purposes.[120, 10] The weakest transitions in the UV-VIS spectral range at 397 and 415 nm remain to be measured directly, but are currently of little relevance to remote sensing. Interestingly, the origin of trends and outliers regarding the symmetry and intensity of transitions within system remain unclear. For example, the transition at 380 nm is symmetric and weaker than the $\Delta\nu_{\rm tot} = 1$ transition. The larger set of transitions at improved SNR available now provide an opportunity to develop theory.

3. Wish list

Similarly to the first HITRAN CIA update [2], inputs from the planetary science and astrophysics communities have been collected and a list of much needed CIA data is presented here. Before discussing in detail the data still missing as requested by the scientific community, it is worth recalling what new data have been produced over the past five years to address the gaps listed in the wish list of the previous update. In that work, CO_2–CO_2, CO_2–CO_2, and CO_2–CH_4 were listed as collision pairs that deserved more detailed studies, especially in the 0-1000 cm^{-1} range. These pairs have been investigated in recent studies [30, 102, 29, 73], and thanks to them, more accurate data will be part of the CIA database with this second update. Moreover, the wish list of the update suggested how the interaction of H_2O with other species deserved further study, especially for early Earth and exoplanet applications: the work of Fluerbaey et al. [25] is a great first step in that direction.

Between the 2019 update and the current release of the HITRAN CIA section, a pivotal advancement has reshaped scientific perspectives in astrophysics and planetary science: the successful launch of JWST, which has enabled observations of astrophysical phenomena and celestial bodies with unprecedented precision. Among other accomplishments, JWST has granted an unprecedented and fast-paced series of discoveries in the field of exoplanets. In particular, with JWST now being the primary instrument for studying exoplanet atmospheres, the new CIA data that would be most valuable to the scientific community are strongly connected to the spectral coverage of JWST. When these atmospheres are studied in Transmission Spectroscopy with NIRISS/NIRSpec, the typical observational range extends from 0.6 to

5.3 µm, with the possibility of extending this range to approximately 10–12 µm for planets with a high signal-to-noise (S/N) ratio, such as Hot Jupiters [128, 129]. In this wavelength range, new CIA binary absorption coefficients should be measured/calculated at different temperatures to match the temperatures of the large variety of atmospheres that can be found outside our Solar System. Regarding hot atmospheres, our knowledge of magma oceans would benefit from CIA data at high temperatures of collisional pairs that can be found in reducing atmospheres (*e.g.,* X-H_2) [130], while our modeling of Venus and Early Earth's atmosphere would benefit from CO_2-X CIA data above 350 K [131], both in the far- and in the mid-infrared. In particular, CO_2-O_2 CIA data up to 700 K could be useful to study planetary atmospheres around M dwarf stars with extended pre-main sequence phase [132].

As already pointed out in the previous wish list, new CIA data for N_2-X (with X=H_2, He, Ne) collisional pairs at even higher temperatures (up to 3000 K) would improve M and brown dwarf stars characterization [133, 134]. In addition, to better characterize these stars, new CIA data at stellar temperatures would help in turn the characterization of exoplanet atmospheres (*Know Thy Star, Know Thy Planet* is the mantra of the exoplanet detection and characterization communities [135]). In fact, stellar contamination has long been recognized as a major bottleneck in transmission spectroscopy, because it could lead to the wrong interpretation of key atmospheric molecular features [136].

4. Conclusions

From Solar System planetary bodies and exoplanets to white and brown dwarfs, collision-induced absorption plays a crucial role in the atmospheric thermal balance of these celestial bodies. To provide a reliable and up-to-date compilation of all the available CIA data reported in literature, the HITRAN CIA section was established in 2012 [1], updated in 2019 [2], and is now undergoing its second update. In this update, new data published over the past five years –including both laboratory measurements and theoretical calculations– have been reviewed, compared, and either incorporated or not into the HITRAN CIA section. This second update became necessary due to the consistent amount of recently published data, most of which published as a response to the data deficiencies highlighted in two previous works. In particular, two collisional pairs, N_2-Ar [26] and CO_2-H_2O [25], have been included in the database for the first time. New data regarding

other collisional pairs already present in the database, including N_2-H_2 [23], CO_2-CO_2 [28], CO_2-H_2 [29], CO_2-CH_4 [30, 29], O_2-O_2 [31], and O_2-CO_2 [32], have been included either because of their improved accuracy or because of their extended frequency or temperature range. Each new database entry is highlighted in Table 1 and is accompanied by a dedicated subsection that discusses the experimental procedure and/or theoretical framework used to produce the data. Despite the remarkable effort to produce new data, the CIA section is still far from being complete: more measurements and calculations are needed, especially at different temperatures. They will be extremely relevant to better interpret current and future observations of exoplanetary atmospheres, which are extremely diverse in terms of constituents and temperature distribution. The new data included in the second update will be made available at www.hitran.org/cia starting INSERT DATE HERE.

Acknowledgments and Funding

The HITRAN2024 edition of the HITRAN database is funded through NASA grants 80NSSC23K1596, and 80NSSC24K0080. This work has been developed under the ASI-INAF agreement n. 2023-6-HH.0. This work was performed in the frame of the ANR project COMPLEAT (ANR-19-CE31-0010-01)

Supplementary material

References

[1] Richard, C. et al, New section of the hitran database: Collision-induced absorption (cia), Journal of Quantitative Spectroscopy and Radiative Transfer 113 (11) (2012) 1276–1285, three Leaders in Spectroscopy. doi:10.1016/j.jqsrt.2011.11.004.

[2] Karman, T. et al, Update of the hitran collision-induced absorption section, Icarus 328 (2019) 160–175. doi:https://doi.org/10.1016/j.icarus.2019.02.034.

[3] Hartmann, J.M. et al, Recent advances in collisional effects on spectra of molecular gases and their practical consequences, Journal of Quantitative Spectroscopy and Radiative Transfer 213 (2018) 178–227. doi:https://doi.org/10.1016/j.jqsrt.2018.03.016.

[4] Mlawer, E., Cady-Pereira, K., Mascio, J. and Gordon, I., The inclusion of the MT_CKD water vapor continuum model in the HITRAN molecular spectroscopic database, Journal of Quantitative Spectroscopy and Radiative Transfer 306 (2023) 108645. doi:10.1016/j.jqsrt.2023.108645.
URL https://doi.org/10.1016/j.jqsrt.2023.108645https://linkinghub.elsevier.com/retrieve/pii/S0022407323001632

[5] Mlawer, E.J. et al, A more transparent infrared window, Journal of Geophysical Research: Atmospheres 129 (2024) e2024JD041366. doi:10.1029/2024JD041366.
URL https://onlinelibrary.wiley.com/doi/full/10.1029/2024JD041366https://onlinelibrary.wiley.com/doi/abs/10.1029/2024JD041366https://agupubs.onlinelibrary.wiley.com/doi/10.1029/2024JD041366

[6] Sioris, C.E. et al, Retrieval of carbon dioxide vertical profiles from solar occultation observations and associated error budgets for ace-fts and cass-fts, Atmospheric Measurement Techniques 7 (2014) 2243–2262. doi:10.5194/amt-7-2243-2014.
URL http://www.atmos-meas-tech.net/7/2243/2014/

[7] Hartmann, J.M., Boulet, C. and Toon, G.C., Collision-induced absorption by n2 near 2.16 μm: Calculations, model, and consequences for atmospheric remote sensing, Journal of Geophysical Research: Atmospheres 122 (4) (2017) 2419–2428. doi:https://doi.org/10.1002/2016JD025677.

[8] Pardo, J.R., Serabyn, E. and Cernicharo, J., Submillimeter atmospheric transmission measurements on Mauna Kea during extremely dry El Nino conditions: implications for broadband opacity contributions, Journal of Quantitative Spectroscopy and Radiative Transfer 68 (2001) 419–433. doi:10.1016/S0022-4073(00)00034-0.

[9] Kiel, M. et al, Improved retrieval of gas abundances from near-infrared solar FTIR spectra measured at the Karlsruhe TCCON station, Atmospheric Meas. Tech. 9 (2) (2016) 669–682. doi:10.5194/amt-9-669-2016.
URL https://www.atmos-meas-tech.net/9/669/2016/

[10] Lauster, B., Frieß, U., Nasse, J.M., Platt, U. and Wagner, T., Assessment of laboratory O_4 absorption cross-sections at 360 nm using atmospheric long-path doas observations, EGUsphere 2025 (2025) 1–23. doi:10.5194/egusphere-2024-3881.

[11] Karman, T. et al, O2- o2 and o2- n2 collision-induced absorption mechanisms unravelled, Nature chemistry 10 (5) (2018) 549–554. doi:https://doi.org/10.1038/s41557-018-0015-x.

[12] Samuelson, R.E., Nath, N.R. and Borysow, A., Gaseous abundances and methane supersaturation in titan's troposphere, Planetary and Space Science 45 (8) (1997) 959–980. doi:https://doi.org/10.1016/S0032-0633(97)00090-1.

[13] Lorenz, R.D., McKay, C.P. and Lunine, J.I., Photochemically driven collapse of titan's atmosphere, Science 275 (5300) (1997) 642–644. doi:10.1126/science.275.5300.642.

[14] Wordsworth, R., Forget, F. and Eymet, V., Infrared collision-induced and far-line absorption in dense CO $_2$ atmospheres, 210 (2) (2010) 992–997. doi:10.1016/j.icarus.2010.06.010.

[15] Ramirez, R.M. et al, Warming early mars with co2 and h2, Nature Geoscience 7 (1) (2014) 59–63. doi:https://doi.org/10.1038/ngeo2000.

[16] Wordsworth, R. et al, Transient reducing greenhouse warming on early mars, Geophysical Research Letters 44 (2) (2017) 665–671. doi:https://doi.org/10.1002/2016GL071766.

[17] Turbet, M. and Tran, H., Comment on "Radiative Transfer in CO_2-Rich Atmospheres: 1. Collisional Line Mixing Implies a Colder Early Mars", Journal of Geophysical Research (Planets) 122 (11) (2017) 2362–2365. arXiv:1711.03376, doi:10.1002/2017JE005373.

[18] Turbet, M. and Forget, F., 3-d global modelling of the early martian climate under a dense co2+h2 atmosphere and for a wide range of surface water inventories (2021). arXiv:2103.10301.
URL https://arxiv.org/abs/2103.10301

[19] Pollack, J.B. et al, Near-infrared light from venus' nightside: A spectroscopic analysis, Icarus 103 (1) (1993) 1–42. doi:https://doi.org/10.1006/icar.1993.1055.

[20] Lebonnois, S., Eymet, V., Lee, C. and Vatant d'Ollone, J., Analysis of the radiative budget of the Venusian atmosphere based on infrared Net Exchange Rate formalism, Journal of Geophysical Research (Planets) 120 (6) (2015) 1186–1200. doi:10.1002/2015JE004794.

[21] Meadows, V.S. et al, Exoplanet biosignatures: Understanding oxygen as a biosignature in the context of its environment, Astrobiology 18 (6) (2018) 630–662. doi:10.1089/ast.2017.1727.

[22] Fauchez, T.J. et al, Sensitive probing of exoplanetary oxygen via mid-infrared collisional absorption, Nature Astronomy 4 (4) (2020) 372–376. doi:https://doi.org/10.1038/s41550-019-0977-7.

[23] Wei, C., Klingberg, A., Strand, C.L. and Hanson, R.K., Measurement of hydrogen and nitrogen via collision-induced infrared absorption, International Journal of Hydrogen Energy 93 (2024) 364–373. doi:https://doi.org/10.1016/j.ijhydene.2024.10.318.

[24] Hübert, T., Boon-Brett, L., Black, G. and Banach, U., Hydrogen sensors – a review, Sensors and Actuators B: Chemical 157 (2) (2011) 329–352. doi:https://doi.org/10.1016/j.snb.2011.04.070.

[25] Fleurbaey, H., Mondelain, D., Fakhardji, W., Hartmann, J. and Campargue, A., Simultaneous collision-induced transitions in h2o+co2 gas mixtures, Journal of Quantitative Spectroscopy and Radiative Transfer 285 (2022) 108162. doi:https://doi.org/10.1016/j.jqsrt.2022.108162.

[26] Serov, E. et al, Continuum absorption in pure n2 gas and in its mixture with ar, Journal of Quantitative Spectroscopy and Radiative Transfer 328 (2024) 109172. doi:https://doi.org/10.1016/j.jqsrt.2024.109172.

[27] Koshelev, M.A. et al, New frontiers in modern resonator spectroscopy, IEEE Transactions on Terahertz Science and Technology 8 (6) (2018) 773–783. doi:10.1109/TTHZ.2018.2875450.

[28] Tran, H., Hartmann, J., Rambinison, E. and Turbet, M., Collision-induced absorptions by pure co2 in the infrared: New measurements in the 1150–4500 cm-1 spectral range and empirical modeling for applications, Icarus 422 (2024) 116265. doi:https://doi.org/10.1016/j.icarus.2024.116265.

[29] Turbet, M., Boulet, C. and Karman, T., Measurements and semi-empirical calculations of co2+ch4 and co2+h2 collision-induced absorption across a wide range of wavelengths and temperatures. application for the prediction of early mars surface temperature, Icarus 346 (2020) 113762. doi:https://doi.org/10.1016/j.icarus.2020.113762.

[30] Fakhardji, W., Boulet, C., Tran, H. and Hartmann, J.M., Direct calculations of the ch4+co2 far infrared collision-induced absorption, Journal of Quantitative Spectroscopy and Radiative Transfer 283 (2022) 108148. doi:https://doi.org/10.1016/j.jqsrt.2022.108148.

[31] Finkenzeller, H. and Volkamer, R., O2–o2 cia in the gas phase: Cross-section of weak bands, and continuum absorption between 297–500 nm, Journal of Quantitative Spectroscopy and Radiative Transfer 279 (2022) 108063. doi:https://doi.org/10.1016/j.jqsrt.2021.108063.

[32] Banerjee, A., Mandon, J., Harren, F. and Parker, D.H., Collision-induced absorption between o2–co2 for the $a^1\delta(\nu = 1) \leftarrow x^3\sigma_g^-(\nu = 0)$ transition of molecular oxygen at 1060 nm, Phys. Chem. Chem. Phys. 21 (2019) 1805–1811. doi:10.1039/C8CP06778C.

[33] Vitali, F. et al, New experimental measurements of the collision induced absorptions of h2-h2 and h2-he in the 3600-5500 cm-1 spectral range from 120 to 500 k, Journal of Quantitative Spectroscopy and Radiative Transfer 330 (2025) 109255. doi:https://doi.org/10.1016/j.jqsrt.2024.109255.

[34] Abel, M., Frommhold, L., Li, X. and Hunt, K.L.C., Collision-induced absorption by h2 pairs: From hundreds to thousands of kelvin, The Journal of Physical Chemistry A 115 (25) (2011) 6805–6812. doi:10.1021/jp109441f.

[35] Fletcher, L.N., Gustafsson, M. and Orton, G.S., Hydrogen dimers in giant-planet infrared spectra, The Astrophysical Journal Supplement Series 235 (1) (2018) 24. doi:10.3847/1538-4365/aaa07a.

[36] Koroleva, A., Kassi, S., Fleurbaey, H. and Campargue, A., The collision-induced absorption of h2 near 1.20 µm: Subatmospheric measurements and validation tests of calculations, Journal of Quantitative Spectroscopy and Radiative Transfer 318 (2024) 108948. doi:https://doi.org/10.1016/j.jqsrt.2024.108948.

[37] Abel, M., Frommhold, L., Li, X. and Hunt, K.L.C., Infrared absorption by collisional h2–he complexes at temperatures up to 9000 k and frequencies from 0 to 20000 cm-1, The Journal of Chemical Physics 136 (4) (2012) 044319. doi:10.1063/1.3676405.

[38] Gustafsson, M. and Frommhold, L., The h2–h infrared absorption bands at temperatures from 1000 k to 2500 k, Astronomy & Astrophysics 400 (3) (2003) 1161–1162. doi:10.1051/0004-6361:20030100.

[39] Gustafsson, M. and Frommhold, L., Infrared absorption spectra of collisionally interacting he and h atoms, The Astrophysical Journal 546 (2) (2001) 1168. doi:10.1086/318311.

[40] Borysow, A. and Frommhold, L., Theoretical Collision-induced Rototranslational Absorption Spectra for the Outer Planets: H2-CH4 Pairs, Astrophysical Journal 304 (1986) 849. doi:10.1086/164221.

[41] Bar-Ziv, E. and Weiss, S., Translational spectra due to collision-induced overlap moments in mixtures of he with co2, n2, ch4, and c2h6, The Journal of Chemical Physics 57 (1) (1972) 34–37. doi:10.1063/1.1677970.

[42] Odintsova, T. et al, Co2–co2 and co2–ar continua at millimeter wavelengths, Journal of Quantitative Spectroscopy and Radiative Transfer 258 (2021) 107400. doi:https://doi.org/10.1016/j.jqsrt.2020.107400.

[43] Taylor, R.H., Borysow, A. and Frommhold, L., Concerning the rototranslational absorption spectra of he-ch4 pairs, Journal of Molecular

Spectroscopy 129 (1) (1988) 45–58. doi:https://doi.org/10.1016/0022-2852(88)90257-3.

[44] Borysow, A. and Frommhold, L., Collision-induced Rototranslational Absorption Spectra of CH4-CH4 Pairs at Temperatures from 50 to 300 K, Astrophysical Journal 318 (1987) 940. doi:10.1086/165426.

[45] Gruszka, M. and Borysow, A., Roto-translational collision-induced absorption of co2for the atmosphere of venus at frequencies from 0 to 250 cm-1, at temperatures from 200 to 800 k, Icarus 129 (1) (1997) 172–177. doi:https://doi.org/10.1006/icar.1997.5773.

[46] Baranov, Y. and Vigasin, A., Collision-induced absorption by co2 in the region of $\nu 1$, $2\nu 2$, Journal of Molecular Spectroscopy 193 (2) (1999) 319–325. doi:https://doi.org/10.1006/jmsp.1998.7743.

[47] Baranov, Y.I., Fraser, G.T., Lafferty, W.J. and Vigasin, A.A., Collision-induced absorption in the co2 fermi triad for temperatures from 211k to 296 k, in: Camy-Peyret, C. and Vigasin, A.A. (Eds.), Weakly Interacting Molecular Pairs: Unconventional Absorbers of Radiation in the Atmosphere, Springer Netherlands, Dordrecht, 2003, pp. 149–158. doi:10.1007/978-94-010-0025-3_12.

[48] Baranov, Y.I., Collision-induced absorption in the region of the $\nu 2+\nu 3$ band of carbon dioxide, Journal of Molecular Spectroscopy 345 (2018) 11–16. doi:https://doi.org/10.1016/j.jms.2017.11.005.

[49] Borysow, A. and Frommhold, L., Theoretical Collision-induced Rototranslational Absorption Spectra for Modeling Titan's Atmosphere: H 2–N 2 Pairs, Astrophysical Journal 303 (1986) 495. doi:10.1086/164096.

[50] Chistikov, D.N., Finenko, A.A., Lokshtanov, S.E., Petrov, S.V. and Vigasin, A.A., Simulation of collision-induced absorption spectra based on classical trajectories and ab initio potential and induced dipole surfaces. i. case study of n2–n2 rototranslational band, The Journal of Chemical Physics 151 (19) (2019) 194106. doi:10.1063/1.5125756.

[51] Baranov, Y., Lafferty, W. and Fraser, G., Investigation of collision-induced absorption in the vibrational fundamental bands of o2 and n2

899 at elevated temperatures, Journal of Molecular Spectroscopy 233 (1)
900 (2005) 160–163. doi:https://doi.org/10.1016/j.jms.2005.06.
901 008.

902 [52] Lafferty, W.J., Solodov, A.M., Weber, A., Olson, W.B. and Hartmann,
903 J.M., Infrared collision-induced absorption by n2 near 4.3μm for at-
904 mospheric applications: measurements and empiricalmodeling, Appl.
905 Opt. 35 (30) (1996) 5911–5917. doi:10.1364/AO.35.005911.

906 [53] Sung, K. et al, Progress in the measurement of temperature-dependent
907 N_2-N_2 collision-induced absorption and H_2-broadening of cold and hot
908 CH_4, Vol. 48 of AAS/Division for Planetary Sciences Meeting Ab-
909 stracts, 2016, p. 424.11.

910 [54] Moreau, G., Étude en température et modélisation de l'absorption in-
911 duite par collision dans les régions des bandes fundamentales pour
912 les mélanges des gaz n_2-ar et o_2, Ph.D. thesis, Université de Rennes
913 (1999).

914 [55] Baranov, Y.I., Lafferty, W. and Fraser, G., Infrared spectrum of the
915 continuum and dimer absorption in the vicinity of the o2 vibrational
916 fundamental in o2/co2 mixtures, Journal of Molecular Spectroscopy
917 228 (2) (2004) 432–440, special Issue Dedicated to Dr. Jon T. Hougen
918 on the Occasion of His 68th Birthday. doi:https://doi.org/10.
919 1016/j.jms.2004.04.010.

920 [56] Mondelain, D., Kassi, S. and Campargue, A., Accurate labora-
921 tory measurement of the o2 collision-induced absorption band near
922 1.27 μm, Journal of Geophysical Research: Atmospheres 124 (1)
923 (2019) 414–423. doi:https://doi-org.sid2nomade-2.grenet.fr/
924 10.1029/2018JD029317.

925 [57] Kassi, S. et al, Temperature dependence of the collision-induced ab-
926 sorption band of o2 near 1.27 νm, Journal of Geophysical Research:
927 Atmospheres 126 (13) (2021) e2021JD034860. doi:https://doi.org/
928 10.1029/2021JD034860.

929 [58] Spiering, F.R. and van der Zande, W.J., Collision induced absorption
930 in the $a^1\delta(\nu = 2) \leftarrow x^3\sigma_g^-(\nu = 0)$ band of molecular oxygen, Phys.
931 Chem. Chem. Phys. 14 (2012) 9923–9928. doi:10.1039/C2CP40961E.

[59] Tran, H., Boulet, C. and Hartmann, J.M., Line mixing and collision-induced absorption by oxygen in the a band: Laboratory measurements, model, and tools for atmospheric spectra computations, Journal of Geophysical Research: Atmospheres 111 (D15) (2006). doi:https://doi.org/10.1029/2005JD006869.

[60] Spiering, F.R., Kiseleva, M.B., Filippov, N.N., van Kesteren, L. and van der Zande, W.J., Collision-induced absorption in the o2 b-band region near 670 nm, Phys. Chem. Chem. Phys. 13 (2011) 9616–9621. doi:10.1039/C1CP20403C.

[61] Thalman, R. and Volkamer, R., Temperature dependent absorption cross-sections of o2–o2 collision pairs between 340 and 630 nm and at atmospherically relevant pressure, Phys. Chem. Chem. Phys. 15 (2013) 15371–15381. doi:10.1039/C3CP50968K.

[62] Thibault, F. et al, Infrared collision-induced absorption by o2near 6.4 µm for atmospheric applications: measurements and empiricalmodeling, Appl. Opt. 36 (3) (1997) 563–567. doi:10.1364/AO.36.000563.

[63] Orlando, J.J., Tyndall, G.S., Nickerson, K.E. and Calvert, J.G., The temperature dependence of collision-induced absorption by oxygen near 6 μm, Journal of Geophysical Research: Atmospheres 96 (D11) (1991) 20755–20760. doi:https://doi.org/10.1029/91JD02042.

[64] Menoux, V., Doucen, R.L., Boulet, C., Roblin, A. and Bouchardy, A.M., Collision-induced absorption in the fundamental band of n2: temperature dependence of the absorption for n2–n2 and n2–o2 pairs, Appl. Opt. 32 (3) (1993) 263–268. doi:10.1364/AO.32.000263.

[65] Drouin, B.J. et al, Multispectrum analysis of the oxygen a-band, Journal of Quantitative Spectroscopy and Radiative Transfer 186 (2017) 118–138, satellite Remote Sensing and Spectroscopy: Joint ACE-Odin Meeting, October 2015. doi:https://doi.org/10.1016/j.jqsrt.2016.03.037.

[66] Hartmann, J.M., Boulet, C., Tran, D.D., Tran, H. and Baranov, Y., Effect of humidity on the absorption continua of co2 and n2 near 4 μm: Calculations, comparisons with measurements, and consequences for

atmospheric spectra, The Journal of Chemical Physics 148 (5) (2018). doi:https://doi.org/10.1063/1.5019994.

[67] Finenko, A.A. et al, Trajectory-based simulation of far-infrared collision-induced absorption profiles of ch4–n2 for modeling titan's atmosphere, The Astrophysical Journal Supplement Series 258 (2) (2022) 33. doi:10.3847/1538-4365/ac36d3.

[68] Borysow, A. and Tang, C., Far infrared cia spectra of n2-ch4 pairs for modeling of titan's atmosphere, Icarus 105 (1) (1993) 175–183. doi:https://doi.org/10.1006/icar.1993.1117.

[69] Vangvichith, M., Tran, H. and Hartmann, J.M., Line-mixing and collision induced absorption for o2–co2 mixtures in the oxygen a-band region, Journal of Quantitative Spectroscopy and Radiative Transfer 110 (18) (2009) 2212–2216. doi:https://doi.org/10.1016/j.jqsrt.2009.06.002.

[70] Snels, M., Stefani, S., Boccaccini, A., Biondi, D. and Piccioni, G., A simulation chamber for absorption spectroscopy in planetary atmospheres, Atmospheric Measurement Techniques 14 (2021) 7187–7197. doi:10.5194/amt-14-7187-2021.

[71] Bouanich, J., Brodbeck, C., Nguyen-Van-Thanh and Drossart, P., Collision-induced absorption by h2-h2 and h2-he pairs in the fundamental band—an experimental study, Journal of Quantitative Spectroscopy and Radiative Transfer 44 (4) (1990) 393–403. doi:https://doi.org/10.1016/0022-4073(90)90120-U.

[72] Brodbeck, C., Nguyen-Van-Thanh, Jean-Louis, A., Bouanich, J.P. and Frommhold, L., Collision-induced absorption by h_2 pairs in the fundamental band at 78 and 298 k, Phys. Rev. A 50 (1994) 484–488. doi:10.1103/PhysRevA.50.484.

[73] Mondelain, D., Boulet, C. and Hartmann, J.M., The binary absorption coefficients for h2+co2 mixtures in the 2.12–2.35 μm spectral region determined by crds and by semi-empirical calculations, Journal of Quantitative Spectroscopy and Radiative Transfer 260 (2021) 107454. doi:https://doi.org/10.1016/j.jqsrt.2020.107454.

[74] Mondelain, D., de Casson, L.B., Fleurbaey, H., Kassi, S. and Campargue, A., Accurate absolute frequency measurement of the s(2) transition in the fundamental band of h2 near 2.03 μm, Phys. Chem. Chem. Phys. 25 (2023) 22662–22668. doi:10.1039/D3CP03187J.

[75] Borysow, A., Collision-induced absorption coefficients of h2 pairs at temperatures from 60 k to 1000 k, Astronomy & Astrophysics 390 (2) (2002) 779–782.

[76] Brodbeck, C., Bouanich, J.P., Van-Thanh, N. and Borysow, A., The binary collision-induced first overtone band of gaseous hydrogen, AIP Conference Proceedings 559 (1) (2001) 433–435. doi:10.1063/1.1370678.

[77] Kassi, S. and Campargue, A., Electric quadrupole transitions and collision-induced absorption in the region of the first overtone band of h2 near 1.25μm, Journal of Molecular Spectroscopy 300 (2014) 55–59, spectroscopic Tests of Fundamental Physics. doi:https://doi.org/10.1016/j.jms.2014.03.022.

[78] Brodbeck, C., Nguyen-Van-Thanh, Bouanich, J.P. and Frommhold, L., Collison-induced absorption by h_2-he pairs in the h_2 fundamental band at 78 and 298 k, Phys. Rev. A 51 (1995) 1209–1213. doi:10.1103/PhysRevA.51.1209.

[79] Hunt, J.L. and Welsh, H.L., Analysis of the Profile of the Fundamental Infrared Band of Hydrogen in Pressure-Induced Absorption, Canadian Journal of Physics 42 (5) (1964) 873–885. doi:10.1139/p64-082.

[80] Finenko, A.A., Accurate neural-network-based fitting of full-dimensional N_2 –Ar and N_2–CH_4 two-body potential energy surfaces aimed at spectral simulations, Molecular Physics 123 (1) (2025) e2348110. arXiv:2210.09970, doi:10.1080/00268976.2024.2348110.

[81] Dore, P. and Filabozzi, A., On the nitrogen-induced far-infrared absorption spectra, Canadian Journal of Physics 65 (1987) 90–93. doi:10.1139/p87-016.

[82] Ryzhov, V., The rotational–translational spectra of N_2 and CO_2 and their mixtures with argon, Physics & Astronomy International Journal 2 (4) (2018) 323–328.

[83] Reddy, S.P. and Cho, C.W., Induced infrared absorption of nitrogen and nitrogen – foreign gas mixtures, Canadian Journal of Physics 43 (12) (1965) 2331–2343. doi:10.1139/p65-223.
URL http://dx.doi.org/10.1139/p65-223

[84] Shapiro, M.M. and Gush, H.P., The collision-induced fundamental and first overtone bands of oxygen and nitrogen, Canadian Journal of Physics 44 (5) (1966) 949–963. doi:10.1139/p66-079.
URL http://dx.doi.org/10.1139/p66-079

[85] Buontempo, U., Filabozzi, A. and Maselli, P., Collision induced fundamental band of n2and n2-ar mixtures, Molecular Physics 67 (3) (1989) 517–523. doi:10.1080/00268978900101261.
URL http://dx.doi.org/10.1080/00268978900101261

[86] Bader, J.S. and Berne, B.J., Quantum and classical relaxation rates from classical simulations, Journal of Chemical Physics 100 (11) (1994) 8359–8366. doi:10.1063/1.466780.

[87] Schofield, P., Space-Time Correlation Function Formalism for Slow Neutron Scattering, Physical Review Letters 4 (5) (1960) 239–240. doi:10.1103/PhysRevLett.4.239.

[88] Chouqar, J. et al, Surface pressure impact on nitrogen-dominated USP super-Earth atmospheres, Monthly Notices of the Royal Astronomical Society 522 (1) (2023) 648–659. arXiv:2304.08690, doi:10.1093/mnras/stad1034.

[89] Miguel, Y., Observability of molecular species in a nitrogen-dominated atmosphere for 55 Cancri e, Monthly Notices of the Royal Astronomical Society 482 (3) (2019) 2893–2901. arXiv:1809.08230, doi:10.1093/mnras/sty2803.

[90] Finenko, A.A., Chistikov, D.N., Kalugina, Y.N., Conway, E.K. and Gordon, I.E., Fitting potential energy and induced dipole surfaces of the van der Waals complex CH_4–N_2 using non-product quadrature

grids, Physical Chemistry Chemical Physics (Incorporating Faraday Transactions) 23 (34) (2021) 18475–18494. doi:10.1039/D1CP02161C.

[91] Frommhold, L., Collision Induced Absorption in Gases, Cambridge University Press, Cambridge, 2006.

[92] Bézard, B. and Vinatier, S., On the H_2 abundance and ortho-to-para ratio in Titan's troposphere, Icarus 344 (2020) 113261. arXiv:1909.10458, doi:10.1016/j.icarus.2019.03.038.

[93] Jennings, D.E. et al, Composite infrared spectrometer (CIRS) on Cassini, Applied Optics 56 (18) (2017) 5274. doi:10.1364/ao.56.005274.

[94] Anderson, C.M. and Samuelson, R.E., Titan's aerosol and stratospheric ice opacities between 18 and 500 μm: Vertical and spectral characteristics from Cassini CIRS, Icarus 212 (2) (2011) 762–778. doi:10.1016/j.icarus.2011.01.024.

[95] Dagg, I.R. et al, Collision-induced absorption in gaseous mixtures of nitrogen and methane., Canadian Journal of Physics 64 (1986) 1467–1474. doi:10.1139/p86-260.

[96] Birnbaum, G., Borysow, A. and Buechele, A., Collision-induced absorption in mixtures of symmetrical linear and tetrahedral molecules: Methane-nitrogen, Journal of Chemical Physics 99 (5) (1993) 3234–3243. doi:10.1063/1.465132.

[97] Johnson, R.M., Bernath, P.F., Billinghurst, B. and Zhao, J., Collision-induced absorption spectra of n2 and ch4, The Astrophysical Journal 979 (2) (2025) 149. doi:10.3847/1538-4357/ada24a.

[98] Tonkov, M.V. et al, Measurements and empirical modeling of pure co2 absorption in the 2.3-μm region at room temperature: far wings, allowed and collision-induced bands, Applied Optics 35 (1996) 4863–4870. doi:https://doi.org/10.1364/AO.35.004863.

[99] Fakhardji, W., Tran, H., Pirali, O. and Hartmann, J.M., Room temperature measurements of the collision-induced absorption by h2+co2

mixtures near 2.4 μm, Journal of Quantitative Spectroscopy and Radiative Transfer 283 (2022) 108161. doi:https://doi.org/10.1016/j.jqsrt.2022.108161.

[100] Wordsworth, R.D., The climate of early mars, Annual Review of Earth and Planetary Sciences 44 (Volume 44, 2016) (2016) 381–408. doi:https://doi.org/10.1146/annurev-earth-060115-012355.

[101] Gruszka, M. and Borysow, A., New analysis of the spectral moments of collision induced absorption in gaseous N2 and CO2 , Molecular Physics 88 (5) (1996) 1173–1185. doi:10.1080/00268979609484502.

[102] Turbet, M. et al, Far infrared measurements of absorptions by ch4+co2 and h2+co2 mixtures and implications for greenhouse warming on early mars, Icarus 321 (2019) 189–199. doi:https://doi.org/10.1016/j.icarus.2018.11.021.

[103] Hellmann, R., Bich, E. and Vesovic, V., Cross second virial coefficients and dilute gas transport properties of the (ch4+co2), (ch4+h2s), and (h2s+co2) systems from accurate intermolecular potential energy surfaces, The Journal of Chemical Thermodynamics 102 (2016) 429–441. doi:https://doi.org/10.1016/j.jct.2016.07.034.

[104] Li, X., Champagne, M.H. and Hunt, K.L.C., Long-range, collision-induced dipoles of Td–Dinfh molecule pairs: Theory and numerical results for CH4 or CF4 interacting with H2, N2, CO2, or CS2, The Journal of Chemical Physics 109 (19) (1998) 8416–8425. doi:10.1063/1.477504.

[105] Bastien, L.A.J., Price, P.N. and Brown, N.J., Intermolecular potential parameters and combining rules determined from viscosity data, International Journal of Chemical Kinetics 42 (12) (2010) 713–723. doi:https://doi.org/10.1002/kin.20521.

[106] Borysow, A. and Tang, C., Far infrared cia spectra of n2-ch4 pairs for modeling of titan's atmosphere, Icarus 105 (1) (1993) 175–183. doi:https://doi.org/10.1006/icar.1993.1117.

[107] Ma, Q. and Tipping, R., A far wing line shape theory and its application to the foreign-broadened water continuum absorption. iii,

The Journal of chemical physics 97 (2) (1992) 818–828. doi:https://doi.org/10.1063/1.463184.

[108] Turbet, M. et al, The environmental effects of very large bolide impacts on early Mars explored with a hierarchy of numerical models, 335 (2020) 113419. arXiv:1902.07666, doi:10.1016/j.icarus.2019.113419.

[109] Pluriel, W., Marcq, E. and Turbet, M., Modeling the albedo of Earth-like magma ocean planets with H_2O-CO_2 atmospheres, 317 (2019) 583–590. arXiv:1809.02036, doi:10.1016/j.icarus.2018.08.023.

[110] Baranov, Y.I., On the significant enhancement of the continuum-collision induced absorption in h2o+ co2 mixtures, Journal of Quantitative Spectroscopy and Radiative Transfer 175 (2016) 100–106. doi:https://doi.org/10.1016/j.jqsrt.2016.02.017.

[111] Tran, H., Turbet, M., Chelin, P. and Landsheere, X., Measurements and modeling of absorption by co2+ h2o mixtures in the spectral region beyond the co2 ν3-band head, Icarus 306 (2018) 116–121. doi:https://doi.org/10.1016/j.icarus.2018.02.009.

[112] Fleurbaey, H. et al, Characterization of the h2o+ co2 continuum within the infrared transparency windows, Journal of Quantitative Spectroscopy and Radiative Transfer 282 (2022) 108119. doi:https://doi.org/10.1016/j.jqsrt.2022.108119.

[113] Tran, H. et al, The co2–broadened h2o continuum in the 100–1500 cm-1 region: Measurements, predictions and empirical model, Journal of Quantitative Spectroscopy and Radiative Transfer 230 (2019) 75–80. doi:https://doi.org/10.1016/j.jqsrt.2019.03.016.

[114] Fleurbaey, H., Reed, Z.D., Adkins, E.M., Long, D.A. and Hodges, J.T., High accuracy spectroscopic parameters of the 1.27 μm band of o2 measured with comb-referenced, cavity ring-down spectroscopy, Journal of Quantitative Spectroscopy and Radiative Transfer 270 (2021) 107684. doi:https://doi.org/10.1016/j.jqsrt.2021.107684.

[115] Maté, B., Lugez, C., Fraser, G.T. and Lafferty, W.J., Absolute intensities for the o2 1.27 μm continuum absorption, Journal of Geophysical

Research: Atmospheres 104 (D23) (1999) 30585–30590. doi:https://doi.org/10.1029/1999JD900824.

[116] Adkins, E.M., Karman, T., Campargue, A., Mondelain, D. and Hodges, J.T., Parameterized model to approximate theoretical collision-induced absorption band shapes for o2-o2 and o2-n2, Journal of Quantitative Spectroscopy and Radiative Transfer 310 (2023) 108732. doi:https://doi.org/10.1016/j.jqsrt.2023.108732.

[117] Absorption cross-sections of atmospheric constituents: No_2, o_2, and h_2o, Environ. Sci. Pollut. Res. 6 (1999) 151–158. doi:10.1007/BF02987620.

[118] Greenblatt, G.D., Orlando, J.J., Burkholder, J.B. and Ravishankara, A.R., Absorption measurements of oxygen between 330 and 1140 nm, J. Geophys. Res. Atmos. 95 (1990) 18577–18582. doi:10.1029/JD095iD11p18577.

[119] Dianov-Klokov, V.I., Absorption spectrum of condensed oxygen in the 1.26–0.3 μm region, Opt. Spectrosc. (1964) 530–534.

[120] Dimitropoulou, E. et al, Horizontal distribution of tropospheric no_2 and aerosols derived by dual-scan multi-wavelength multi-axis differential optical absorption spectroscopy (max-doas) measurements in uccle, belgium, Atmospheric Measurement Techniques 15 (2022) 4503–4529. doi:10.5194/amt-15-4503-2022.

[121] Lampel, J. et al, Detection of o_4 absorption around 328 and 419 nm in measured atmospheric absorption spectra, Atmos. Chem. Phys. 18 (2018) 1671–1683. doi:10.5194/acp-18-1671-2018.

[122] Koenig, T.K. et al, Troposphere–stratosphere-integrated bromine monoxide (bro) profile retrieval over the central pacific ocean, Atmospheric Measurement Techniques 17 (2024) 5911–5934. doi:10.5194/amt-17-5911-2024.

[123] Lee, C.F. et al, Elevated tropospheric iodine over the central continental united states: Is iodine a major oxidant of atmospheric mercury?, Geophysical Research Letters 51 (2024) e2024GL109247, e2024GL109247 2024GL109247. doi:https://doi.org/10.1029/2024GL109247.

[124] Nowlan, C.R. et al, Global formaldehyde products from the ozone mapping and profiler suite (omps) nadir mappers on suomi npp and noaa-20, Earth and Space Science 10 (2023) e2022EA002643, e2022EA002643 2022EA002643. doi:https://doi.org/10.1029/2022EA002643.

[125] Lee, G.T. et al, First evaluation of the gems formaldehyde product against tropomi and ground-based column measurements during the in-orbit test period, Atmospheric Chemistry and Physics 24 (2024) 4733–4749. doi:10.5194/acp-24-4733-2024.

[126] Kwon, H.A. et al, Updated omi glyoxal column measurements using collection 4 level 1b radiances, Earth and Space Science 11 (2024) e2024EA003705. doi:https://doi.org/10.1029/2024EA003705.

[127] Zhao, R. et al, First satellite observation of total column water vapor from the chinese environmental trace gases monitoring instrument, Science China Earth Sciences 68 (2025) 977–997. doi:10.1007/s11430-023-1418-8.

[128] Kendrew, S. et al, The mid-infrared instrument for the james webb space telescope, iv: The low-resolution spectrometer, Publications of the Astronomical Society of the Pacific 127 (953) (2015) 623. doi:10.1086/682255.

[129] Jakobsen, P. et al, The near-infrared spectrograph (nirspec) on the james webb space telescope - i. overview of the instrument and its capabilities, A&A 661 (2022) A80. doi:10.1051/0004-6361/202142663.

[130] Nicholls, H., Lichtenberg, T., Bower, D.J. and Pierrehumbert, R., Magma ocean evolution at arbitrary redox state, Journal of Geophysical Research: Planets 129 (12) (2024) e2024JE008576. doi:https://doi.org/10.1029/2024JE008576.

[131] Lee, Y.J. et al, Sensitivity of net thermal flux to the abundance of trace gases in the lower atmosphere of venus, Journal of Geophysical Research: Planets 121 (9) (2016) 1737–1752. doi:https://doi.org/10.1002/2016JE005087.

[132] Luger, R. and Barnes, R., Extreme water loss and abiotic o2 buildup on planets throughout the habitable zones of m dwarfs, Astrobiology 15 (2) (2015) 119–143. doi:10.1089/ast.2014.1231.

[133] Trafton, L.M., Planetary Atmospheres: the Role of Collision-Induced Absorption, pp. 177–193. doi:10.1142/9789812812155_0006.

[134] Trampedach, R., A modelers' opacity wish list (2018). arXiv:1804.04123.
URL https://arxiv.org/abs/1804.04123

[135] Fauchez, T.J., Rackham, B.V., Ducrot, E., Stevenson, K.B. and de Wit, J., Stellar models also limit exoplanet atmosphere studies in emission (2025). arXiv:2502.19585.

[136] Rackham, B.V. and de Wit, J., Toward robust corrections for stellar contamination in jwst exoplanet transmission spectra, The Astronomical Journal 168 (2) (2024) 82. doi:10.3847/1538-3881/ad5833.